Analysis of enhanced β effects in minimal flavor violation GUT scenarios

Enrico Lunghi[*]

Fermi National Accelerator Laboratory, P.O. Box 500, Batavia, Illinois 60510-0500, USA

Werner Porod[†]

IFIC - Instituto de Física Corpuscular, CSIC, E-46071, València, Spain

Oscar Vives[‡]

Departament de Física Teòrica and IFIC, Universitat de València-CSIC, E-46100, Burjassot, Spain
(Received 10 July 2006; published 12 October 2006)

We analyze a minimal supersymmetric standard model (MSSM) taking a minimal flavor violation structure at the GUT scale. We evaluate the parameters at the electroweak scale taking into account the full flavor structure in the evolution of the renormalization group equations. We concentrate mainly on the decay $B_s \to \mu^+ \mu^-$ and its correlations with other observables like BR($b \to s\gamma$), BR($b \to sl^+l^-$), ΔM_{B_s} and the anomalous magnetic moment of the muon. We restrict our analysis to the regions in parameter space consistent with the dark matter constraints. We find that the BR($B_s \to \mu^+ \mu^-$) can exceed the current experimental limit in the regions of parameter space which are allowed by all other constraints thus providing an additional bound on supersymmetric parameters. This holds even in the constrained MSSM. Assuming a hypothetical measurement of BR($B_s \to \mu^+ \mu^-$) $\simeq 10^{-7}$, we analyze the predicted MSSM spectrum and flavor violating decay modes of supersymmetric particles which are found to be small.

I. INTRODUCTION

The minimal supersymmetric standard model (MSSM) is the simplest supersymmetric (SUSY) structure that includes the SM gauge group and matter content. However, this definition does not unambiguously fix a single supersymmetric model. As is well known, SUSY cannot be an exact symmetry of nature and must be broken. Therefore, to specify completely the model, it is necessary to fix the soft-breaking terms: this amounts to 124 parameters at the electroweak scale. Although these parameters would be fixed in the presence of a truly fundamental theory, from the point of view of the effective theory they are only constrained by low energy experimental data. In fact, our freedom in this enormous parameter space is already severely limited by phenomenological constraints. The accumulating concordance between the SM expectations and the vast range of experimental results in FCNC and *CP* violation point toward a low energy new physics which is, at least approximately, flavor blind [1]. In this spirit, the so-called minimal flavor violating (MFV) MSSM is a MSSM where the only nontrivial flavor structures present are the usual Yukawa couplings while all sfermion masses and trilinear couplings are completely family universal [2]. Notice that realistic flavor models have been constructed where the deviations from this minimal flavor structure are rather small [3].

Several interesting flavor-changing processes can take place for large values of $\tan\beta$ at a rate much larger than the corresponding expectations from the SM. A particularly interesting process in this scenario is the decay $B_s \to \mu^+ \mu^-$ which has been shown to receive enhancements of even 3 orders of magnitude with respect to the standard model expectations for large $\tan\beta$ and small pseudoscalar Higgs masses [4,5]. This process has been carefully analyzed in previous studies. In fact, two different points of view have been taken in these analyses. On the one hand, several groups examined this decay in the framework of an effective MFV MSSM model defined at the electroweak scale where masses and mixing angles are uncorrelated [6–12]. In these works, large enhancement factors are relatively easy to find because several correlations with other observables are lost. On the other hand, various other works repeated this analysis in a MFV MSSM defined at the GUT scale in terms of a reduced number of parameters [5,13–22]. Most of these analyses take place in the framework of a constrained MSSM (CMSSM) defined at $M_{\rm GUT}$ in terms of m_0, $m_{1/2}$, A_0, $\tan\beta$, and sgn(μ) and neglecting flavor mixing in the RGE evolution. In principle it is possible to consider different family-universal masses for different representations under the gauge group. However, to our knowledge, in the literature so far only the masses of the Higgs multiplets are allowed to be different from a common sfermion mass [23–25] with the only exception being Ref. [26]. In any of these GUT scenarios, several relations between the sfermion masses, gaugino masses, Higgs masses, and mixing angles are obtained and although large enhancements of the $B_s \to \mu^+ \mu^-$ branch-

[*]Electronic address: lunghi@fnal.gov
[†]Electronic address: porod@ific.uv.es
[‡]Electronic address: oscar.vives@uv.es

ing ratio are still allowed, they are clearly more difficult to obtain.

In this work we analyze this decay in the framework of a completely generic MFV MSSM defined at the GUT scale. In this general MFV scenario, the soft masses and trilinear terms for different representations under the SM gauge group are different, although family universal. This scenario can be realized in different ways—as RGE-induced splittings between different multiplets in the running from M_{Planck} to M_{GUT} in $SU(5)$ or flipped $SU(5)$ models [27] or in models of direct unification at the Planck scale [28]. Another difference with respect to previous analysis is the fact that, for the first time, we use the full two-loop renormalization group equations (RGE) [29] with the complete flavor structure of the different flavor matrices to determine the Yukawa couplings and soft SUSY breaking parameters at the electroweak scale. Furthermore, we take into account all the relevant constraints in our analysis including the dark matter relic abundance [30] together with the updated results on processes like $B_s - \bar{B}_s$ mixing [31,32], muon anomalous magnetic moment [33], $b \to sl^+l^-$ [34,35], and the LEP and Tevatron constraints from searches of SUSY particles [36]. All the analysis is done with updated values of the input parameters and, in particular, we use the last value of the top quark mass [37]. Finally, we take into account the latest constraints on the BR($B_s \to \mu^+\mu^-$) from the D0 and CDF collaborations [38]. In this framework, we study the neutral Higgs effects in the decay $B_s \to \mu^+\mu^-$ and the B_s mass difference, comparing the results of the CMSSM with our generic MFV scenario. We take special care in checking the compatibility of these processes with other $\tan\beta$ enhanced observables like the $b \to s\gamma$ decay or the muon anomalous magnetic moment.

For completeness, we want to note that in Ref. [12] a related study was performed with a slightly different definition of MFV which is defined at the electroweak scale. They also consider a nonminimal flavor violating scenario where the off-diagonality in the neutral gaugino vertices at the electroweak scale is still proportional to the Cabibbo-Kobayashi-Maskawa quark-mixing matrix (CKM). This additional term can be generated for instance due to RGE effects and is closely related to our definition of MFV at the GUT scale within the CMSSM. In these two scenarios they also analyze $B_s \to \mu^+\mu^-$, $\Delta(M_{B_s})$, $b \to s\gamma$, kaon physics, and neutral Higgs boson physics. We have found agreement with respect to their results on $B_s \to \mu^+\mu^-$, $\Delta(M_{B_s})$, $b \to s\gamma$ which are also covered in this paper. In addition we consider these observables in an extended model and include also $b \to sl^+l^-$, the dark matter constraint, and also discuss predictions for future collider experiments, e.g. the Large Hadron Collider (LHC), yielding complementary results to the ones of Ref. [12].

The structure of the paper is as follows: We start with a discussion of the origin of Higgs-mediated flavor-changing neutral currents (FCNC) and study their phenomenological effects in the $B_s \to \mu^+\mu^-$ decay and the B_s mass difference which are enhanced by additional $\tan\beta$ factors. In Sec. III we analyze the correlations of these Higgs-mediated processes with other $\tan\beta$ enhanced observables like the $b \to s\gamma$ decay, the muon anomalous magnetic moment, and the $b \to sl^+l^-$ decay. In Sec. IV we describe the procedure used in our numerical analysis and present our results for the $B_s \to \mu^+\mu^-$ decay in the various scenarios. Furthermore, we discuss the various correlations with other observables. Section V is devoted to the discussion of the expected collider phenomenology if the decay $B_s \to \mu^+\mu^-$ is found with a branching ratio close to the present bounds. Finally, in Sec. VI we present our conclusions.

II. HIGGS-MEDIATED FCNC'S

The MSSM is classically a type II two-Higgs doublet model. This means that one of the Higgs fields, H_u, couples only to the up quarks while the other, H_d, couples only to the down quarks. In this way, dangerous tree-level Higgs-mediated FCNC's are avoided. However, the presence of the μ term in the superpotential breaks the symmetry protecting this structure. Therefore quantum corrections modify this type II structure and generate couplings of $H_d^\dagger$ to up quarks and of $H_u^\dagger$ to down quarks, hence reintroducing Higgs-mediated FCNC's. We use in our numerical analysis the full expressions for the one-loop vertex and self-energy corrections as given in Ref. [10] (see also [39]). All our numerical results are valid for any value of $\tan\beta$. However, in the following we summarize the main features of Higgs-mediated FCNCs, relevant for our analysis, in the limit of large $\tan\beta$. A more detailed discussion can be found in Ref. [10]. In Fig. 1 we present an example of FCNC coupling of the up-type Higgs, H_u, to the down quarks through a stop-chargino loop. There are also similar couplings mediated by gluino loops and the corresponding H_d couplings to up quarks. The effective Yukawa Lagrangian at one-loop is
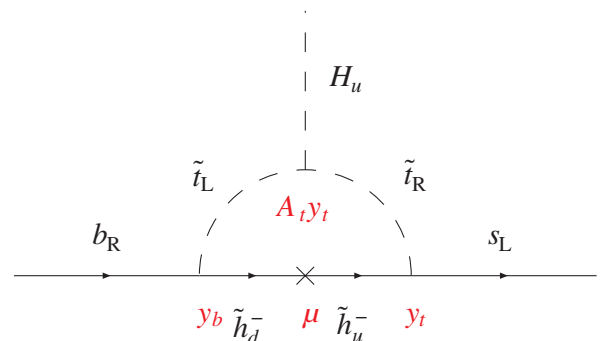

FIG. 1 (color online). Flavor-changing coupling of the up Higgs boson, H_u, to the down-type quarks.

$$\mathcal{L}_{\text{Yuk}} = -\bar{d}_{L_i} Y^d_{ij} d_{R_j} H_d + \bar{d}_{L_i} (\Delta Y^d)_{ij} d_{R_j} H^*_u$$
$$+ \bar{u}_{L_i} Y^u_{ij} u_{R_j} H_u + \bar{u}_{L_i} (\Delta Y^u)_{ij} u_{R_j} H^*_d, \quad (1)$$

where Y^d_{ij} and Y^u_{ij} include also the one-loop corrections to the H_d down quark and H_u up quark couplings [10]. After spontaneous breaking of the electroweak symmetry, this Lagrangian gives rise to new contributions to the quark mass matrices. Working in the basis where the tree-level down quark Yukawa couplings are diagonal and neglecting the subdominant loop corrections in the large $\tan\beta$ limit, the contributions to the down quark mass matrix are

$$\mathcal{L}^d_{\text{mass}} = -\bar{d}_{L_i} \left(Y^d_{ii} \delta_{ij} \frac{v_d}{\sqrt{2}} + (\Delta Y^d)_{ij} \frac{v_u}{\sqrt{2}} \right) d_{R_j} + \text{H.c.}$$
$$= \frac{v_d}{\sqrt{2}} \bar{d}_{L_i} (Y^d_{ii} \delta_{ij} + \tan\beta (\Delta Y^d)_{ij}) d_{R_j} + \text{H.c.}, \quad (2)$$

where we can see the appearance of a $\tan\beta$ enhanced correction to the down quark mass due to the presence of the wrong type Higgs vacuum expectation value. In the same basis, we obtain for the neutral Higgs couplings to the down quarks [10]:

$$\mathcal{L}_{S^0} = -\bar{d}_{L_i} \left(\frac{\bar{m}_{d_j}}{v_d(1 + \tilde{\epsilon}_j \tan\beta)} x^S_d \delta_{ij} + (\Delta Y^d)_{ij} x^S_u \right) d_{R_j} S^0$$
$$+ \text{H.c.}, \quad (3)$$

with $S^0 = (H^0, h^0, A^0, G^0)$, $x^S_d = (\cos\alpha, -\sin\alpha, i\sin\beta, -i\cos\beta)$, and $x^S_u = (\sin\alpha, \cos\alpha, -i\cos\beta, -i\sin\beta)$. Here, $\bar{m}_j$ denotes the running quark mass that can be extracted by experiments, the parameter $\tilde{\epsilon}_j$ accounts for the $\tan\beta$ enhanced corrections to the down quark eigenvalues [10,39] and it is given by

$$\tilde{\epsilon}_j = \epsilon_0 + |K_{3j}|^2 y^2_t \epsilon_Y,$$
$$\epsilon_0 = -2\alpha_s \frac{\mu}{3\pi m_{\tilde{g}}} H_2\left(\frac{m^2_{\tilde{d}_L}}{m^2_{\tilde{g}}}, \frac{m^2_{\tilde{d}_R}}{m^2_{\tilde{g}}} \right),$$
$$\epsilon_Y = \frac{A_t}{16\pi^2 \mu} H_2\left(\frac{m^2_{\tilde{t}_L}}{\mu^2}, \frac{m^2_{\tilde{t}_R}}{\mu^2} \right), \quad (4)$$

where the loop function is defined in Appendix D. Using the fact that[1] $H_2(1,1) = -1/2$ and taking the limit $m_{\tilde{g}} \simeq \mu \simeq m_{\tilde{t}_a} \simeq -A_t$, we obtain $\epsilon_0 \simeq \text{sign}(\mu) \cdot 0.012$ and $\tilde{\epsilon}_3 \simeq \text{sign}(\mu) \cdot 0.015$. Finally $(\Delta Y^d)_{ij}$ is given by

$$(\Delta Y^d)_{ij} = y_{d_j}(\epsilon_0 \delta_{ij} + y^2_t K^*_{3i} K_{3j} \epsilon_Y), \quad (5)$$

with y_{d_j} being the eigenvalues of the tree-level Yukawa matrix.

After diagonalizing the full one-loop down quark mass matrix, the couplings to the neutral Higgs bosons are given by

$$\mathcal{L}_{S^0} = -\bar{d}_{L_i} \left(\frac{\bar{m}_{d_j}}{v_d(1 + \tilde{\epsilon}_j \tan\beta)} (x^S_d + \tilde{\epsilon}_j x^S_u) \delta_{ij} \right.$$
$$\left. + \frac{\bar{m}_{d_j}}{v_d(1 + \tilde{\epsilon}_j \tan\beta)^2} y^2_t \lambda^{ij}_0 \epsilon_Y (x^S_u - x^S_d \tan\beta) \right) d_{R_j} S^0$$
$$+ \text{H.c.}, \quad (6)$$

with $\lambda^{ii}_0 = 0$ and $\lambda^{ij}_0 = K^*_{3i} K_{3j}$. Hence, from this equation we can see that we do have Higgs-mediated FCNC's after the diagonalization of the one-loop mass matrix and in particular $\tan\beta$ enhanced off-diagonal couplings proportional to x^S_d which come from the rotation diagonalizing the one-loop Yukawa couplings. In the following we study the phenomenological consequences of these FCNC Higgs couplings in the down quark sector.[2]

A. The decay $B_s \rightarrow \mu^+\mu^-$

The present experimental bound on this decay from the CDF and D0 [38,48] collaborations is

$$\text{BR}(B_s \rightarrow \mu^+\mu^-) < 1.0 \times 10^{-7} \qquad 95\%\text{C.L.} \quad (7)$$

This process is specially sensitive to the presence of Higgs-mediated FCNC's. Using the Lagrangian given in Eq. (6) we obtain the dominant $\tan\beta$-enhanced neutral Higgs terms to this decay which contribute mainly through two effective operators:

$$\mathcal{H}_{\text{eff}} = -\frac{2G_F}{\sqrt{2}} \frac{\alpha}{2\pi\sin^2\theta_W} K^*_{tb} K_{ts} [C_S \bar{m}_b(\bar{b}_R s_L)(\bar{l}l)$$
$$+ C_P \bar{m}_b(\bar{b}_R s_L)(\bar{l}\gamma_5 l)]. \quad (8)$$

The dominant contributions to the Wilson coefficients C_S and C_P in the large $\tan\beta$ limit are

$$C_S \simeq \frac{m_\mu \bar{m}^2_t}{4M^2_W} \frac{A_t \tan^3\beta H_2(m^2_{\tilde{t}_L}/\mu^2, m^2_{\tilde{t}_R}/\mu^2)}{\mu(1 + \epsilon_0 \tan\beta)(1 + \tilde{\epsilon}_3 \tan\beta)}$$
$$\times \left[\frac{\sin(\alpha - \beta)\cos\alpha}{M^2_{H^0}} - \frac{\cos(\alpha - \beta)\sin\alpha}{M^2_{h^0}} \right], \quad (9)$$

$$C_P \simeq -\frac{m_\mu \bar{m}^2_t}{4M^2_W} \frac{A_t \tan^3\beta H_2(m^2_{\tilde{t}_L}/\mu^2, m^2_{\tilde{t}_R}/\mu^2)}{\mu(1 + \epsilon_0 \tan\beta)(1 + \tilde{\epsilon}_3 \tan\beta)} \left[\frac{1}{M^2_A} \right].$$

For large $\tan\beta$ we can neglect the $M^2_{h^0}$ contribution and, taking $M_{H^0} \simeq M_A$, we find that[3] $C_S \simeq C_P$. Therefore, the leading contribution to the $b_R s_L \rightarrow \mu^+\mu^-$ amplitude is given by

---

[1]We have that $H_2(x, x)$ goes from -0.18 for $x = 4$ to -1.7 for $x = 0.1$.

[2]Other papers study the large $\tan\beta$ effects in τ decays [40–42], flavor-changing decays of the Higgs bosons [43,44] and collider processes [45–47].

[3]However, a difference between these masses is possible for light pseudoscalar Higgs and can give rise to sizable effects [41,42,49]. In our numerical calculation, we use the full expression and we have found that for $M_A \gtrsim 250$ GeV, $C_S \simeq C_P$ is a very good approximation.

$$\mathcal{A}(b_R s_L \to \mu^+ \mu^-)$$

$$\propto \bar{m}_t^2 \frac{\bar{m}_b m_\mu K_{tb}^* K_{ts}}{(1 + \epsilon_0 \tan\beta)(1 + \tilde{\epsilon}_3 \tan\beta)} \frac{A_t}{\mu}$$

$$\times \frac{\tan^3\beta}{M_A^2} H_2(m_{t_L}^2/\mu^2, m_{t_R}^2/\mu^2). \quad (10)$$

Using this formula, we obtain an estimate of the branching ratio in the large $\tan\beta$ region as

$$\text{BR}(B_s \to \mu^+\mu^-) = 2.2 \times 10^{-6} \left[\frac{\tau_{B_s}}{1.5 \text{ ps}}\right] \left[\frac{F_{B_s}}{230 \text{ MeV}}\right]^2$$

$$\times \left[\frac{\bar{m}_t}{175 \text{ GeV}}\right]^4 \left[\frac{\tan\beta}{50}\right]^6 \left[\frac{350 \text{ GeV}}{M_A}\right]^4$$

$$\times \frac{A_t^2}{\mu^2} \frac{(H_2(m_{t_L}^2/\mu^2, m_{t_R}^2/\mu^2))^2}{(1 + \epsilon_0 \tan\beta)^2(1 + \tilde{\epsilon}_3 \tan\beta)^2}, \quad (11)$$

and we see that the branching ratio for this decay scales like $\tan^6\beta/m_A^4$. As we will show below, given the new experimental bounds from CDF and D0, this process is already able to probe a sizable part of the large $\tan\beta$ parameter space.

B. $B_{d,s}^0$ mass differences

The CDF and D0 collaborations [32] have recently presented the first experimental results on B_s mass difference:

$$\Delta M_{B_s} = (17.33^{+0.42}_{-0.21}(\text{stat}) \pm 0.07(\text{syst})) \text{ ps}^{-1}, \quad (12)$$

while the B_d mass difference is

$$\Delta M_{B_d} = (0.500^{+0.42}_{-0.21}(\text{stat}) \pm 0.07(\text{syst})) \text{ ps}^{-1}. \quad (13)$$

The basic formula for the B_q mass difference is [10]

$$\Delta M_{B_q} = \frac{G_F^2 M_W^2}{6\pi} M_{B_q} \eta_B F_{B_q}^2 \hat{B}_{B_q} |K_{tq}|^2 |F_{tt}^q|, \quad (14)$$

with

$$F_{tt}^q = \left[S_0(m_t^2/M_W^2) + \frac{1}{4r} C_{\text{new}}^{\text{VLL}}(\mu) \right] + \frac{1}{4r} C_1^{\text{VRR}}(\mu)$$

$$+ \bar{P}_1^{LR} C_1^{LR}(\mu) + \bar{P}_2^{LR} C_2^{LR}(\mu) + \bar{P}_1^{\text{SLL}}[C_1^{\text{SLL}}(\mu)$$

$$+ C_1^{\text{SRR}}(\mu)] + \bar{P}_2^{\text{SLL}}[C_2^{\text{SLL}}(\mu) + C_2^{\text{SRR}}(\mu)]. \quad (15)$$

The different Wilson coefficients are defined in [10] and $r = 0.985$ describes the $O(\alpha_s)$ radiative corrections to $S_0(m_t^2/M_W^2)$ in the SM.

As shown in Refs. [10,50], the same flavor-changing Higgs couplings generating the leading contribution to the decay $B_s \to \mu^+\mu^-$ at large $\tan\beta$ induce a Higgs-mediated double-penguin contribution to $B_{s,d} - \bar{B}_{s,d}$ mixing. In the large $\tan\beta$ regime, the dominant contributions to the $B_{s,d}$ mass differences are given by the usual SM box and by the double-penguin contribution

$$\Delta M_{B_q} \propto |K_{tq}|^2 \left[S_0(m_t^2/M_W^2) - \frac{\sqrt{2}G_F}{\pi^2 M_W^2} \right.$$

$$\times \frac{\bar{m}_b \bar{m}_q m_t^4}{(1 + \epsilon_0 \tan\beta)^2(1 + \tilde{\epsilon}_3 \tan\beta)^2} \frac{A_t^2 \tan^4\beta}{\mu^2 m_A^2}$$

$$\left. \times (H_2(m_{t_L}^2/\mu^2, m_{t_R}^2/\mu^2))^2 \right], \quad (16)$$

with $q = s$, d, and $S_0(x)$ defined in the appendices. From this expression we can see that the double-penguin contribution is suppressed by an additional factor of G_F with respect to the SM contribution due to the fact that it is a two-loop contribution. However, it has a strong dependence on $\tan\beta$ which can lead to a huge enhancement compensating this loop suppression. Moreover, these double-penguin contributions have always opposite sign with respect to the standard model box contribution and thus reduce the mass difference for large $\tan\beta$. This effect is specially important in the case of ΔM_{B_s} yielding an additional constraint in the large $\tan\beta$ regime. Notice that in the case of ΔM_{B_d}, the double-penguin contribution is the same as in ΔM_{B_s} with an additional suppression of m_d/m_s. Given that this contribution competes with the same SM function $S_0(x_t)$, it is clear that this process will not be relevant to constrain the SUSY contributions.

III. CORRELATIONS WITH OTHER PROCESSES

Given the strong dependence of $B_s \to \mu^+\mu^-$ on m_A and $\tan\beta$, we can expect that other processes, especially $\tan\beta$ dependent processes, receive large SUSY contributions if $\text{BR}(B_s \to \mu^+\mu^-)$ is at the 10^{-7} level. A typical example is the decay $B \to X_s\gamma$ whose measured BR agrees very well with the SM prediction. In turn this provides a stringent constraint to SUSY contributions and given that the chargino amplitude is proportional to $\tan\beta$ this holds, in particular, for the large $\tan\beta$ regime. The decay $B \to X_s\ell^+\ell^-$ is closely related and the combination of both processes has been recently shown to eliminate the possibility of changing the sign of the dipole Wilson coefficient C_7 in MFV scenarios [51,52]. Another important constraint is provided by the muon anomalous magnetic moment a_μ which is also $\tan\beta$ dependent and constitutes a very important constraint specially for $\mu < 0$.

A. $B \to X_s\gamma$

The standard model contributions to the decay $B \to X_s\gamma$ are known at next-to-leading order (NLO) [53,54] and the excellent agreement with the experimental results constrain strongly any extension of the SM. Charged Higgs contributions in two-Higgs doublet models are also known at NLO [53,55,56]. In the MSSM a complete NLO calculation is still missing but the most important contributions have been calculated in Refs. [57–60]. The MSSM contributes to this process mostly through the dipole operators

$$H_{\text{Dipole}}^{b \to s\gamma} = -\frac{4G_F}{\sqrt{2}} K_{tb}^{\text{eff}} K_{ts}^{\text{eff}*} \left[C_7(\mu) \cdot \frac{e\bar{m}_b}{16\pi^2} \bar{s}_L \sigma_{\mu\nu} b_R F^{\mu\nu} \right.$$
$$\left. + C_8(\mu) \cdot \frac{g_s \bar{m}_b}{16\pi^2} \bar{s}_{L\alpha} T_{\alpha\beta}^a \sigma_{\mu\nu} b_{R\beta} G^{a\mu\nu} \right]. \quad (17)$$

The experimental world average from the CLEO [61], Belle [62,63], and *BABAR* [64,65] collaborations is given by [66]

$$\text{BR}\,(B \to X_s\gamma)_{E_\gamma > 1.6\,\text{GeV}}$$
$$= (3.55 \pm 0.24^{0.09}_{-0.10} \pm 0.03) \times 10^{-4}. \quad (18)$$

This has to be compared with the standard model prediction [67]

$$\text{BR}[\bar{B} \to X_s\gamma] = \left(3.61 \genfrac{}{}{0pt}{}{+0.24}{-0.40} \Big|_{m_c/m_b} \pm 0.02_{\text{CKM}} \right.$$
$$\left. \pm 0.24_{\text{param}} \pm 0.14_{\text{scale}} \right) \times 10^{-4}. \quad (19)$$

In the numerical analysis we utilize the formula presented in Ref. [67] in which the branching ratio is explicit given in terms of arbitrary complex C_7 and C_8.

The two Wilson coefficients, $C_7(\mu)$ and $C_8(\mu)$, receive contributions from W-boson, charged Higgs, and chargino diagrams. It is very interesting to discuss the relative signs of these three contributions. Charged Higgs and W-boson diagrams have the same sign and interfere always constructively. In contrast, the chargino contribution can have either sign depending on the sign of the μ parameter. In the large $\tan\beta$ region the relative sign of the chargino mediated diagram is given by $-\text{sign}(A_t\mu)$. In the scenarios studied in this paper $\text{sign}(A_t) = -\text{sign}(M_{1/2})$ as can be seen in Table IV of [26]. For this reason, $\mu > 0$ implies destructive interference while $\mu < 0$ implies constructive interference of the chargino and W-boson contributions.

Given that the SM contribution essentially saturates the experimental bound, $\mu < 0$ scenarios are tightly constrained and the sum of charged Higgs and chargino contributions is restricted to be a small correction. However, for positive μ the chargino contribution has opposite sign with respect to the W-boson and charged Higgs ones. In this case, a cancellation between sizable charged Higgs and chargino contributions allows one to keep the total Wilson coefficient within a small margin from the SM expectation. In principle it is possible for the chargino to cancel both the charged Higgs and W-boson contributions and generate a total Wilson coefficient of equal modulus and opposite sign to the usual SM contribution. This is consistent with experimental data because the $\text{BR}(B \to X_s\gamma)$ depends essentially on $|C_7^{\text{eff}}(\mu_b)|^2$ and therefore is not sensitive to the sign of these coefficients. However, as we will see later, combining this process with the decay $B \to X_s \ell^+ \ell^-$, it is possible to constrain the sign of the C_7 Wilson coefficient [51,52] and exclude this possibility in the generic MFV scenarios studied.

The complete expressions for the leading-order contributions to the C_7 and C_8 contributions that are used in our numerical evaluation are well known and can be found in Refs. [68,69]. For the following discussion, it is enough to examine the C_7 coefficient as C_8 behaves in a similar way,

$$C_7^W(m_W) = \frac{m_t^2}{4m_W^2} f_1(m_t^2/m_W^2), \quad (20)$$

$$C_7^{H^+}(m_W) = \frac{1}{6}\left\{ \frac{1}{2} \frac{m_t^2}{m_{H^\pm}^2} \frac{1}{\tan^2\beta} f_1(m_t^2/m_{H^\pm}^2) + f_2(m_t^2/m_{H^\pm}^2) \right.$$
$$\cdot \left(1 - \frac{(\epsilon_0' + \tilde{\epsilon}_3)\tan\beta}{1 + \tilde{\epsilon}_3\tan\beta} \right.$$
$$\left. \left. + y_b^2 y_t^2 \frac{\epsilon_Y \epsilon_Y' \tan^2\beta}{(1 + \tilde{\epsilon}_3\tan\beta)(1 + \epsilon_0\tan\beta)} \right) \right\}, \quad (21)$$

$$C_7^{\tilde{\chi}}(m_W) = \frac{1}{3} \sum_{\alpha,\alpha'} \sum_{i=1}^{2} \sum_{a=1}^{6} \frac{K_{\alpha b}^{\text{eff}} K_{\alpha's}^{\text{eff}*}}{K_{tb}^{\text{eff}} K_{ts}^{\text{eff}*}} \frac{m_W^2}{m_{\tilde{\chi}_I^\pm}^2}$$
$$\times \left\{ -\frac{1}{2} G^{(\alpha',a)I*} G^{(a,\alpha)I} f_1(m_{\tilde{u}_a}^2/m_{\tilde{\chi}_I^\pm}^2) \right.$$
$$+ \frac{m_{\tilde{\chi}_I}}{m_W} \frac{1}{\sqrt{2}\cos\beta(1 + \tilde{\epsilon}_3\tan\beta)} G^{(\alpha',a)I*} H^{(a,\alpha)I}$$
$$\left. \times f_2(m_{\tilde{u}_a}^2/m_{\tilde{\chi}_I^\pm}^2) \right\}, \quad (22)$$

where, for simplicity we have only included in this equation the leading contributions in the limit of unbroken $SU(2) \times U(1)$ symmetry [10]. In the numerical analysis we use the complete expressions with full flavor dependence. The parameters ϵ_0' and ϵ_Y' are given by

$$\epsilon_Y' = \frac{A_b}{16\pi^2\mu} H_2\left(\frac{m_{\tilde{b}_L}^2}{\mu^2}, \frac{m_{\tilde{b}_R}^2}{\mu^2} \right),$$
$$\epsilon_0' = \frac{-2\alpha_s\mu}{3\pi m_{\tilde{g}}} H_2\left(\frac{m_{\tilde{s}_L}^2}{m_{\tilde{g}}^2}, \frac{m_{\tilde{s}_R}^2}{m_{\tilde{g}}^2} \right). \quad (23)$$

The main $\tan\beta$ effects are then present in the charged Higgs couplings and in the chargino couplings to right-handed down squarks. $K_{\alpha q} G^{(\alpha,k)I}$ represents the coupling of the chargino I and the squark k to the left-handed down quark q; and $m_q/(\sqrt{2}m_W\cos\beta)K_{\alpha q}H^{(\alpha,k)i}$ the coupling of the chargino i and of the squark k to the right-handed down quark q. These couplings, in terms of the standard mixing matrices defined in the appendices are [70]

$$G^{(\alpha,k)I} = \left(\Gamma_{UL}^{k\alpha} V_{I1}^* - \frac{m_\alpha}{\sqrt{2}m_W\sin\beta} \Gamma_{UR}^{k\alpha} V_{I2}^* \right) \quad (24)$$
$$H^{(\alpha,k)I} = -U_{I2}\Gamma_{UL}^{k\alpha}.$$

The explicit expressions for the loop functions can be found in the appendices.

In the large $\tan\beta$ regime, it is interesting to expand the $C_7^{\tilde{\chi}}$ coefficient assuming the smallness of the off-diagonal entries with respect to the corresponding diagonal elements both in the stop and chargino (more precisely in $M_{\tilde{\chi}}M_{\tilde{\chi}}^\dagger$) mass matrices. In this approximation we obtain

$$
C_7^{\tilde{\chi}}(m_W) \simeq \frac{-\mu A_t m_t^2}{6m_W^2 \sin^2\beta} \frac{\tan\beta}{1 + \tilde{\epsilon}_3 \tan\beta} \frac{m_W^2}{m_{\tilde{\chi}_2^\pm}^2}
$$
$$
\times \frac{f_2(m_{\tilde{t}_L}^2/m_{\tilde{\chi}_2^\pm}) - f_2(m_{\tilde{t}_R}^2/m_{\tilde{\chi}_2^\pm})}{m_{\tilde{t}_L}^2 - m_{\tilde{t}_R}^2}
$$
$$
\simeq \frac{\mu A_t m_t^2}{6m_W^2 \sin^2\beta} \frac{\tan\beta}{1 + \tilde{\epsilon}_3 \tan\beta} \frac{5m_W^2}{12m_{\tilde{t}}^4}, \qquad (25)
$$

where in the second line we replaced the combination of loop functions by its value in the limit in which stop left, stop right, and chargino have the same "average" SUSY mass, $m_{\tilde{t}}^2$. In this limit the SUSY contribution to the amplitude is

$$
\mathcal{A}(b_R \rightarrow s_L \gamma) \propto \frac{4G_F}{\sqrt{2}} K_{tb}^{\text{eff}} K_{ts}^{\text{eff}*} \bar{m}_b \frac{5\mu A_t m_t^2 \tan\beta}{72 m_{\tilde{t}}^4 (1 + \tilde{\epsilon}_3 \tan\beta)}. \qquad (26)
$$

If we compare now this amplitude with the corresponding amplitude of the $B_s \rightarrow \mu^+\mu^-$ decay, Eq. (10), we see that, although both of them are enhanced by powers of $\tan\beta$, these two amplitudes behave differently: $\mathcal{A}(b_R s_L \rightarrow l^+l^-)$ scales as $\tan^3\beta/m_A^2$ while the $b \rightarrow s\gamma$ amplitude scales as $\tan\beta/m_{\tilde{t}}^2$ (assuming μ, A_t, and $m_{\tilde{t}}$ of the same order). Taking into account this difference we can analyze if it is possible to obtain a large contribution for $B_s \rightarrow \mu^+\mu^-$ while at the same time satisfy the stringent bounds on the $b \rightarrow s\gamma$ decay. Obviously, the answer to this question depends on the sign of μ.

In the $B \rightarrow X_s\gamma$ decay with $\mu < 0$, chargino contributions to C_7 and C_8 have the same sign as charged Higgs and W-boson contributions. If we require a sizable neutral Higgs contribution to $B_s \rightarrow \mu^+\mu^-$, we need a light pseudoscalar Higgs, which implies also a light charged Higgs, and large $\tan\beta$. A light charged Higgs enhances $C_7^{H^+}$ while large $\tan\beta$ enhances $C_7^{\tilde{\chi}}$. As both contributions compete to fill the narrow space left over by the SM contribution in the $B \rightarrow X_s\gamma$ amplitude, these two requirements are clearly incompatible. The only possible solution is to increase the squark masses (in particular the stop mass) to suppress the chargino contribution to C_7 while keeping m_A as low and $\tan\beta$ as large as possible. In this case we are essentially in a two-Higgs doublet model without SUSY and from the existing constraints on the charged Higgs mass [53,55,56] we infer that the pseudoscalar must be equally heavy. Moreover, the constraints from the muon anomalous magnetic moment, that are analyzed below, make the $\mu < 0$ situation even more difficult. Therefore, it is not

possible to reach very large values of $\text{BR}(B_s \rightarrow \mu^+\mu^-)$, as we will see in the numerical analysis of the next section.

The case $\mu > 0$ is much more interesting phenomenologically. A large $\text{BR}(B_s \rightarrow \mu^+\mu^-)$ still requires a light charged Higgs and large $\tan\beta$; however, the chargino contributions interfere now destructively with the charged Higgs and W-boson ones and thus these two conditions are fully compatible because $|C_7^{\tilde{\chi}} + C_7^{H^+}| \lesssim 0.1 C_7^{\text{SM}}$. As we will see in the next section, this cancellation must be quite precise and this constraint remains very strong. In the flavor-blind models defined at the GUT scale, in particular, in the CMSSM, it is not always easy to obtain the required values of m_A, $m_{\tilde{t}}$, and $\tan\beta$ to achieve this cancellation. The extent to which this cancellation can be realized will be addressed in the next section where we perform a full analysis of the parameter space.

B. $B \rightarrow X_s \ell^+ \ell^-$

The effective Hamiltonian that describes $b \rightarrow s\ell\ell$ transitions in the standard model is

$$
H_{\text{eff}} = -\frac{4G_F}{\sqrt{2}} K_{tb}^* K_{ts}^* \left(\sum_{i=1}^{10} C_i(\mu) O_i(\mu) + \sum_{i=3}^{6} C_{iQ}(\mu) O_{iQ}(\mu) + C_b O_b(\mu) \right), \qquad (27)
$$

where we adopt the same definitions as in Ref. [52]. The operators O_{iQ} and O_b are required only for the inclusion of electroweak corrections. In particular, the most relevant Wilson coefficients are $C_2(\mu_b)$ (that does not receive sizable new physics contributions), $C_7(\mu_b)$, $C_8(\mu_b)$, $C_9(\mu_b)$, and $C_{10}(\mu_b)$. The explicit definitions of O_7 and O_8 are given in Eq. (17) and the semileptonic operators read

$$
O_9 = \frac{\alpha_{\text{em}}}{4\pi}(\bar{s}_L \gamma_\mu b_L)(\bar{\ell}\gamma^\mu \ell),
$$
$$
O_{10} = \frac{\alpha_{\text{em}}}{4\pi}(\bar{s}_L \gamma_\mu b_L)(\bar{\ell}\gamma^\mu \gamma_5 \ell). \qquad (28)
$$

The branching ratio $\text{BR}(B \rightarrow X_s\ell\ell)$ is known at next-to-next-to-leading order in QCD and at NLO in QED (only terms enhanced by large logarithms—i.e. $\log m_W/m_b$ and $\log m_b/m_\ell$—are included).

Intermediate $c\bar{c}$ resonances produce peaks in the dilepton invariant mass ($4m_\ell^2 < s < m_B^2$) spectrum and disrupt quark-hadron duality. For this reason one has to consider the low- and high-s regions separately. The very low-s region ($s < 1 \text{ GeV}^2$) is dominated by the quasireal photon emission and contains the same amount of information we already extract from $b \rightarrow s\gamma$. In the high-s region ($s > 14.3 \text{ GeV}^2$) the integrated branching ratio is quite small; moreover, the $1/m_b$ expansion breaks down and reliable predictions for the spectrum suffer large uncertainties. The low-s region ($1 \text{ GeV}^2 < s < 6 \text{ GeV}^2$) is dominated by the Wilson coefficients C_9 and C_{10}, has sizable integrated branching ratio, and is very sensitive to the $C_7 - C_9$ inter-

ference. In the following, we utilize the latter to put constraints on the Wilson coefficients $C_{7,8,9,10}$.

We calculate the integrated branching ratio in the low-s region following Ref. [52]:

$$
\begin{aligned}
\mathrm{BR}_{\ell\ell} = [&2.2306 - 0.0005\,\mathcal{I}(R_{10}) + 0.0005\,\mathcal{I}(R_{10}R_8^*) + 0.0906\,\mathcal{I}(R_7) + 0.0223\,\mathcal{I}(R_7R_8^*) + 0.0050\,\mathcal{I}(R_7R_9^*) \\
&+ 0.0086\,\mathcal{I}(R_8) + 0.0258\,\mathcal{I}(R_8R_9^*) - 0.0615\,\mathcal{I}(R_9) - 0.5389\,\mathcal{R}(R_{10}) + 0.1140\,\mathcal{R}(R_7) + 0.0154\,\mathcal{R}(R_7R_{10}^*) \\
&+ 0.0687\,\mathcal{R}(R_7R_8^*) - 0.8414\,\mathcal{R}(R_7R_9^*) - 0.0036\,\mathcal{R}(R_8) + 0.0019\,\mathcal{R}(R_8R_{10}^*) - 0.0980\,\mathcal{R}(R_8R_9^*) \\
&+ 2.6260\,\mathcal{R}(R_9) - 0.1074\,\mathcal{R}(R_9R_{10}^*) + 10.6042|R_{10}|^2 + 0.2837|R_7|^2 + 0.0039|R_8|^2 + 1.4645|R_9|^2] \times 10^{-7},
\end{aligned}
\tag{29}
$$

where $R_i = C_i^{\mathrm{tot}}(\mu_0)/C_i^{\mathrm{SM}}(\mu_0)$ are the next-to-leading order Wilson coefficients [i.e. they do not include $O(\alpha_s)$ corrections] at the high scale normalized to their SM values. When dealing with the dipole operators we utilize the standard definition of the scheme-independent effective coefficients [52]. In the numerical analysis we set to zero supersymmetric contributions to the NLO matching conditions.

The standard model and supersymmetric contributions to the leading order matching conditions of the semileptonic operators are [52] (we do not give explicit formulas for the gluino, neutralino, and neutral Higgses contributions because their effects are negligible compared to the charged Higgs and chargino ones):

$$
C_9^W = \frac{1}{s_W^2}Y(x_t) + W(x_t) + \frac{4}{9} - \frac{4}{9}\log\frac{\mu_0^2}{m_t^2}, \tag{30}
$$

$$
C_{10}^W = -\frac{1}{s_W^2}Y(x_t), \tag{31}
$$

$$
C_9^{H^\pm} = \frac{4s_W^2 - 1}{8s_W^2}\frac{x_t}{\tan^2\beta}f_5(m_t^2/m_{H^\pm}^2) + \frac{1}{18}\frac{1}{\tan^2\beta}f_6(m_t^2/m_{H^\pm}^2), \tag{32}
$$

$$
C_{10}^{H^\pm} = \frac{1}{8s_W^2}\frac{x_t}{\tan^2\beta}f_5(m_t^2/m_{H^\pm}^2), \tag{33}
$$

$$
\begin{aligned}
C_9^{\tilde{\chi}^\pm} = \sum_{\alpha,\alpha'}\sum_{A,B=1}^{6}\sum_{I,J=1}^{2}\frac{K_{\alpha b}^{\mathrm{eff}}K_{\alpha's}^{\mathrm{eff}*}}{K_{tb}^{\mathrm{eff}}K_{ts}^{\mathrm{eff}*}}G^{(\alpha',A)I*}G^{(B,\alpha)J}\bigg[&\frac{1-4s_W^2}{s_W^2}\Big(c_2(m_{\tilde{\chi}_I^\pm}^2, m_{\tilde{u}_A}^2, m_{\tilde{u}_A}^2)(\Gamma_{UL}\Gamma_{UL}^\dagger)_{AB}\delta_{IJ} \\
&+ \frac{m_{\tilde{\chi}_I}m_{\tilde{\chi}_J}}{2}c_0(m_{\tilde{u}_A}^2, m_{\tilde{\chi}_I^\pm}^2, m_{\tilde{\chi}_J^\pm}^2)\delta_{AB}U_{I1}^*U_{J1} - c_2(m_{\tilde{u}_A}^2, m_{\tilde{\chi}_I^\pm}^2, m_{\tilde{\chi}_J^\pm}^2)\delta_{AB}V_{I1}^*V_{J1}\Big) - \frac{2}{9}\frac{m_W^2}{m_{\tilde{u}_A}^2}f_7(m_{\tilde{\chi}_I^\pm}^2/m_{\tilde{u}_A}^2)\delta_{AB}\delta_{IJ} \\
&+ \frac{2}{s_W^2}m_W^2 d_2(m_{\tilde{\chi}_I^\pm}^2, m_{\tilde{\chi}_J^\pm}^2, m_{\tilde{u}_A}^2, m_{\tilde{\nu}_1}^2)\delta_{AB}V_{I1}^*V_{J1}\bigg],
\end{aligned}
\tag{34}
$$

$$
\begin{aligned}
C_{10}^{\tilde{\chi}^\pm} = -\frac{1}{2s_W^2}\sum_{\alpha,\alpha'}\sum_{A,B=1}^{6}\sum_{I,J=1}^{2}\frac{K_{\alpha b}^{\mathrm{eff}}K_{\alpha's}^{\mathrm{eff}*}}{K_{tb}^{\mathrm{eff}}K_{ts}^{\mathrm{eff}*}}G^{(\alpha',A)I*}G^{(B,\alpha)J}\bigg[&c_2(m_{\tilde{\chi}_I^\pm}^2, m_{\tilde{u}_A}^2, m_{\tilde{u}_A}^2)(\Gamma_{UL}\Gamma_{UL}^\dagger)_{AB}\delta_{IJ} \\
&+ \frac{m_{\tilde{\chi}_I}m_{\tilde{\chi}_J}}{2}c_0(m_{\tilde{u}_A}^2, m_{\tilde{\chi}_I^\pm}^2, m_{\tilde{\chi}_J^\pm}^2)\delta_{AB}U_{I1}^*U_{J1} + [2m_W^2 d_2(m_{\tilde{\chi}_I^\pm}^2, m_{\tilde{\chi}_J^\pm}^2, m_{\tilde{u}_A}^2, m_{\tilde{\nu}_1}^2) - c_2(m_{\tilde{u}_A}^2, m_{\tilde{\chi}_I^\pm}^2, m_{\tilde{\chi}_J^\pm}^2)]\delta_{AB}V_{I1}^*V_{J1}\bigg].
\end{aligned}
\tag{35}
$$

A scan of the CMSSM and MFV parameter space results in tiny deviations of the Wilson coefficients C_9 and C_{10} from their SM values: $|C_9^{\mathrm{SUSY}}/C_9^{\mathrm{SM}}| < 0.3/1.65$ and $|C_{10}^{\mathrm{SUSY}}/C_{10}^{\mathrm{SM}}| < 0.8/4.45$.

This decay has been observed by Belle [34] and *BABAR* [35]. In the low-s region the experimental results read as

$$\mathrm{BR}(B \to X_s\ell^+\ell^-) = (1.493 \pm 0.504^{+0.411}_{-0.321}) \times 10^{-6}$$

$$\text{(Belle)}, \tag{36}$$

$$\mathrm{BR}(B \to X_s\ell^+\ell^-) = (1.8 \pm 0.7 \pm 0.5) \times 10^{-6}$$

$$\text{(BABAR)}. \tag{37}$$

This leads to a world average

$$\mathrm{BR}(B \to X_s\ell^+\ell^-)_{\mathrm{WA}} = (1.60 \pm 0.51) \times 10^{-6}. \tag{38}$$

That is in perfect agreement with the SM prediction, that reads

$$\begin{aligned}
\mathrm{BR}(B \to X_s \ell^+ \ell^-)_{\mathrm{SM}} = [&1.58 \pm 0.07_{\mathrm{scale}} \pm 0.06_{m_t} \\
&\pm 0.025_{m_c} \pm 0.015_{m_b} \\
&\pm 0.023_{\alpha_s(M_Z)} \pm 0.015_{\mathrm{CKM}} \\
&\pm 0.025_{\mathrm{BR_{sl}}}] \times 10^{-6} \\
= (&1.58 \pm 0.10) \times 10^{-6}.
\end{aligned} \tag{39}$$

In order to assess the impact of this measurement on the supersymmetric parameter space, we perform a model-independent analysis. As a first step we extract the allowed ranges for the Wilson coefficients C_7 and C_8 from the measured $B \to X_s \gamma$ branching fraction. This gives two thin stripes in the $C_7 - C_8$ plane that correspond to the $C_7 < 0$ and $C_7 > 0$ scenarios. We further restrict C_8 to be within a factor of 10 around the SM value. As a second step, we consider the two strips separately, vary C_7 and C_8 in the allowed range, and plot the resulting constraint in the $C_9 - C_{10}$ plane. The whole analysis is performed at the 90% C.L. and theory errors are included. Our results are summarized in Fig. 2. The most striking feature of these plots is that, in the $C_7 > 0$ scenario, the SM point is excluded and contributions in MFV supersymmetric scenarios are not large enough to bring theory and experiment into agreement; thus we conclude that in such models the sign of C_7 has to be SM-like (i.e. negative). For a similar discussion, see also [51].

C. Muon anomalous magnetic moment

In SUSY theories, a_{μ^+} receives contributions via vertex diagrams with $\tilde{\chi}^0 - \tilde{\mu}$ and $\tilde{\chi}^\pm - \tilde{\nu}$ loops [71]. The chargino diagram strongly dominates in almost all the parameter space. For simplicity, we will present here only the dominant part of the chargino contribution (the complete expressions that we use in the numerical simulation can be found in Ref. [71]):

$$\delta a^{\tilde{\chi}\tilde{\nu}}_{\mu^+} \simeq -\frac{g_2^2}{8\pi^2} \frac{m_\mu^2}{m_{\tilde{\nu}}^2} \sum_{i=1}^{2} \frac{m_{\tilde{\chi}_i} \operatorname{Re}(U_{i2} V_{i1})}{\sqrt{2} M_W \cos\beta} f_3\left(\frac{m_{\tilde{\chi}_i}^2}{m_{\tilde{\nu}}^2}\right), \tag{40}$$

where the loop function f_3 is given in the appendices. In fact, if we expand this function in the small off-diagonal elements of the chargino matrix, we obtain for the dominant $\tan\beta$ enhanced contribution

$$\delta a^{\tilde{\chi}\tilde{\nu}}_{\mu^+} \simeq \frac{g_2^2}{32\pi^2} \frac{m_\mu^2}{m_{\tilde{\nu}}^2} \frac{\operatorname{Re}(\mu) M_2 \tan\beta}{m_{\tilde{\nu}}^2}, \tag{41}$$

where we have chosen the convention $M_2 > 0$ as we do in the rest of the paper. The most relevant feature of Eqs. (40) and (41) is that the sign of $\delta a^{\tilde{\chi}\tilde{\nu}}_{\mu^+}$ is fixed by $\operatorname{sign}[\operatorname{Re}(U_{12} V_{11})] = -\operatorname{sign}[\operatorname{Re}(\mu)]$. The experimental result for this observable is at present [72],

$$a_\mu^{\exp} = 11\,659\,208\,(6) \times 10^{-10}, \tag{42}$$

while the theoretical expectations within the SM are [73],

$$\begin{aligned}
a_\mu^{\mathrm{SM}}(e^+ e^-) &= 11\,659\,181\,(8) \times 10^{-10}, \\
a_\mu^{\mathrm{SM}}(\tau) &= 11\,659\,196\,(7) \times 10^{-10}.
\end{aligned} \tag{43}$$

Comparison with the experimental results implies that these results strongly favor the $\mu > 0$ region in a MFV scenario. This is especially true for the theoretical prediction based on $e^+ e^-$ annihilation that is smaller than the experimental result by 2.7σ. In the case of the prediction based on τ decay, the difference is reduced to 1.4σ [72] but it still requires a positive correction and disfavors strongly a sizable negative contribution. Therefore, this has important consequences in all our observables. As we saw in the previous section, $\mu > 0$ is precisely the phenomenologically interesting region for the combination of the $B_s \to \mu^+ \mu^-$ and $B \to X_s \gamma$ decays. On the other hand the a_μ measurement makes it even more difficult to find interesting effects in $B_s \to \mu^+ \mu^-$ for $\mu < 0$. In the numerical
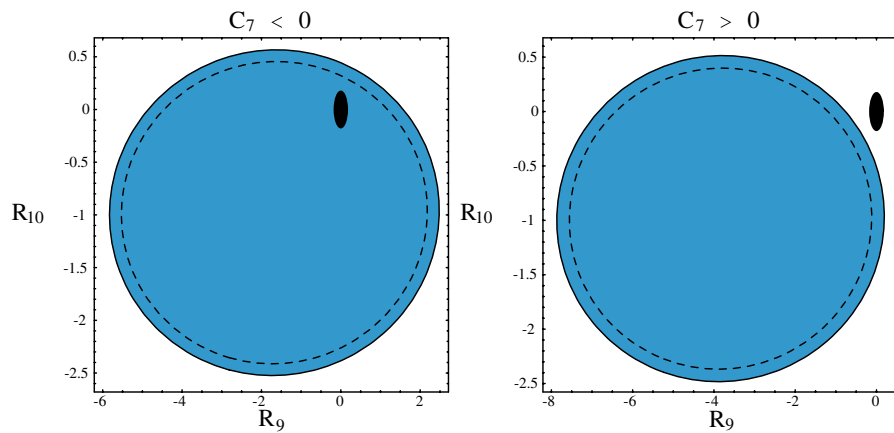

FIG. 2 (color online). Impact of the $\mathrm{BR}(B \to X_s \ell\ell)$ measurement on the $R_9 - R_{10}$ plane. The black disk is the region accessible in an MFV model, i.e. it includes the possible SUSY contributions both in the CMSSM as in the generic MFV scenario that we analyze here.

analysis, presented in the next section, we use a conservative a_μ bound at 3σ with the $e^+ e^-$ based estimate of the SM contribution, and we still find that with $\mu < 0$ we can only find BR($B_s \rightarrow \mu^+ \mu^-$) at the level of 10^{-8} with a very heavy SUSY spectrum. In the $\mu > 0$ region, the conservative 3σ bound allows for a vanishing supersymmetric contribution.

IV. NUMERICAL RESULTS

As said in the introduction, in this work we concentrate on a version of the MSSM with MFV soft-breaking terms at the GUT scale. This means that the only nontrivial flavor structures in the model are the usual SM Yukawa couplings; all soft-breaking masses are family universal and the trilinear couplings are proportional to the corresponding Yukawa matrices. The RGE evolution between the GUT and electroweak scales introduces small nonuniversal entries in the soft-breaking terms.

In this framework we analyze two different versions of the MSSM: the CMSSM and the most general MFV MSSM. The full spectrum of the CMSSM is determined (assuming vanishing SUSY phases) by five parameters: $M_{1/2}$, m_0, A_0, $\tan\beta$, and sign(μ). Therefore, the SUSY parameters at the electroweak scale, including couplings, masses, and mixing angles, show several interesting correlations. Furthermore, these five parameters are strongly constrained by the experimental bounds on masses and different FCNC processes. In this restricted framework it is very interesting to investigate how large BR($B_s \rightarrow \mu^+ \mu^-$) $\propto \tan^6\beta/m_A^4$ can be, while remaining in agreement with all the other experimental constraints.

We can ask the same question in a more general flavor-blind MSSM, where we allow for different, but generation-diagonal, parameters for the fields with different gauge quantum numbers. Here the number of parameters is 13: $M_{1/2}$, $m_{\tilde{Q},0}$, $m_{\tilde{u}_R,0}$, $m_{\tilde{d}_R,0}$, $m_{\tilde{L},0}$, $m_{\tilde{e}_R,0}$, $m_{H_d,0}$, $m_{H_u,0}$, $A_{u,0}$, $A_{d,0}$, $A_{e,0}$, $\tan\beta$, and sign(μ), where 0 in the subscripts indicates that these parameters are defined at $M_{\rm GUT}$. The precise definition of $M_{\rm GUT}$ and the numerical evaluation of the parameters at the electroweak scale will be described below. Clearly, in this model we have more freedom than in the CMSSM, implying milder correlations between the masses of different particles; thus, we can expect larger rates for the Higgs-mediated processes consistent with other FCNC constraints.

In the numerical analysis presented below we define our model, CMSSM or most general MFV, in terms of the GUT scale parameters listed above. We scan the values of these parameters in the following ranges: $M_{1/2} \leq 1$ TeV, $m_{i,0} \leq 2$ TeV ($i = Q$, u_R, d_R, L, e_R, H_u, H_d), $A_{u,0}^2 \leq 3(m_{\tilde{Q},0}^2 + m_{\tilde{u}_R,0}^2 + m_{H_u,0}^2)$, $A_{d,0}^2 \leq 3(m_{\tilde{Q},0}^2 + m_{\tilde{d}_R,0}^2 + m_{H_d,0}^2)$, $A_{e,0}^2 \leq 3(m_{\tilde{L},0}^2 + m_{\tilde{e}_R,0}^2 + m_{H_d,0}^2)$; $|\mu|$ is calculated from the requirement of correct electroweak symmetry breaking.

The bound on the $A_{i,0}$ parameters is set to avoid charge and/or color breaking minima.

At the low scale, we impose the following constraints on each point:

  (i) Lower bound on the light and pseudoscalar Higgs masses [74];
 (ii) the LEP constraints on the lightest chargino and sfermion masses [36];
(iii) the LEP and Tevatron constrains on squarks and gluino masses [36];
(iv) agreement with the experimental data on low energy processes like BR($B \rightarrow X_s \gamma$), δa_μ, BR($B_s \rightarrow \mu^+ \mu^-$), BR($B \rightarrow X_s \ell^+ \ell^-$), ΔM_{B_s} [31–35,38,48,61–65];
 (v) correct dark matter relic abundance from stable neutralinos [30].[4]

We consider MSSM with conserved R parity and thus, the lightest neutralino (that coincides with the lightest supersymmetric particle) provides an excellent dark matter candidate. In fact, the recent precise determination of the cold dark matter density of the Universe is a very strong constraint on the SUSY parameter space. In most of the parameter space of the MSSM the neutralino abundance generates a too large density of cold dark matter. Only certain regions of the parameter space, in which neutralinos are efficiently annihilated, are in agreement with the experimental results.

The most precise results on the cold dark matter density come from the WMAP experiment [30]:

$$\Omega_{\rm CDM} h^2 = 0.1047^{+0.007}_{-0.013} \quad \text{at } 68\% \text{C.L.} \qquad (44)$$

This constraint selects very narrow strips in the MSSM parameter space [75]. On the other hand it has been shown [76] that these allowed regions are extremely sensitive to small differences in the computation of SUSY masses. This is especially true in the large $\tan\beta$ region that we analyze in this paper, where differences in the stability of radiative symmetry breaking or in the Higgs masses are due to the different approximations used in the RGE programs. In view of all this, we prefer to take a conservative attitude with respect to the dark matter constraint and, allowing the possibility of other cold dark matter candidates, impose only the loose 99% C.L. upper bound,

$$\Omega_{\rm CDM} h^2 \leq 0.13. \qquad (45)$$

In this section we analyze the different parameters (masses, mixing matrices, ...) that enter the $B_s \rightarrow \mu^+ \mu^-$ amplitude and the impact of the various constraints that we have discussed above. We start with the analysis of this process in the CMSSM and then generalize it to the most general MFV model at the GUT scale.

---

[4]This constraint assumes a standard thermal history of the Universe and can be evaded easily in nonstandard cosmological models.

A. Calculation of the parameters at the electroweak scale

In the numerical calculations, we use the following procedure. The masses and mixing angles at the electroweak scale are calculated in an iterative way: First the gauge and Yukawa couplings are calculated from the input values given in Table I at the electroweak scale taking into account the shift from the $\overline{\text{MS}}$ to the $\overline{\text{DR}}$ scheme as well as the effect of the SUSY thresholds. In case of the SUSY thresholds the complete flavor structure of the sfermions is taken into account in the calculation. Afterward these couplings are evolved to the GUT scale which is defined by the requirement $g_1 = g_2$ where $g_1 = \sqrt{5/3}g'$ is the properly normalized $U(1)$ coupling and g_2 is the $SU_L(2)$ coupling. We do not require at M_{GUT} that g_3 is equal to $g_1 = g_2$ but assume that this differences is accounted for by unknown thresholds due to very heavy particles with masses of the order M_{GUT}. At M_{GUT} the SUSY breaking boundary conditions are set. At this scale the trilinear couplings are obtained multiplying the A parameters with the Yukawa matrices taking into account the *complete* flavor structure. Also in the RGE evolution, the complete flavor structure is taken into account and we evolve the parameters at the two-loop order [29]. This clearly induces off-diagonal elements in the sfermion mass parameters. The calculation of the SUSY masses is carried out in the $\overline{DR}$ scheme and the formulas for the one-loop masses are generalizations of the ones given in Ref. [77] taking into account the complete flavor structure and will be presented elsewhere [78]. In the case of the μ parameter and the masses of the neutral Higgs bosons the two-loop corrections as given in Refs. [79–84] are added. Note that in the one-loop contributions we use the full flavor structure, while for the two-loop part we use the approximation that only the sfermions of the third generation contribute. The obtained spectrum is then used to recalculate the thresholds to gauge and Yukawa couplings restarting the complete procedure. This is repeated until the relative difference of all couplings and masses between subsequent iterations is at most 10^{-5}.

The calculation of the Yukawas, in particular Y_d, is important for the calculation of low energy observables. In the calculation of the Yukawa couplings [see Eq. (1)] we take into account the thresholds of supersymmetric particles as given in [10]. Because of the RGE running, off-diagonal elements in the squark sector are induced which remain nonzero when going to the super-CKM basis. For this reason, not only the chargino contributions to the off-diagonal terms but also gluino and neutralino contributions are taken into account although the later ones are negligible. The gluino contribution amounts typically to a 10% correction of the chargino contribution, which is precisely the order of magnitude one would expect for the two-loop corrections.

For the calculation of the low energy observables, the complete formulas are used, including all contributions stemming from H^+, $\tilde{\chi}_i^\pm$, $\tilde{\chi}_j^0$, $\tilde{g}$, h^0, H^0, A^0 in case of B physics observables and the contributions due to $\tilde{\chi}_i^\pm$, $\tilde{\chi}_j^0$ in case of a_μ. More precisely, in case of $B_s \rightarrow \mu^+ \mu^-$ we combine the formulas of [10,85,86]. However, we use only the lowest order contributions to C_S, C_P, C_S', C_P', C_{10}, and C_{10}' because the complete one-loop QCD corrections to these Wilson coefficients are not available in the literature. In the case of ΔM_{B_q} we have used the formulas of Refs. [10,87]. In the case of $b \rightarrow s\gamma$ we have used the formulas given in [69] and we have added the leading SM QCD corrections as described in [67]. For the SUSY contributions to the anomalous magnetic moment of the muon we have used the formulas given in [88]. The hadronic parameters we use in all these calculations are collected in Table II. In most of the cases we neglect the uncertainty in these parameters with the exception of $f_{B_s} \hat{B}_{B_s}^{1/2}$ that has a large impact in the B_s mass difference. In the calculation of the B_s mass difference we compare below the results obtained fixing this parameter to the value in Table II and the results varying $f_{B_s} \hat{B}_{B_s}^{1/2}$ within the one-sigma range $f_{B_s} \hat{B}_{B_s}^{1/2} = (0.295 \pm 0.036)$ GeV [90].

B. $B_s \rightarrow \mu^+ \mu^-$ in the CMSSM

As we have seen in previous sections, $\tan\beta$ enhanced Higgs FCNC at low energies are inversely proportional to the pseudoscalar Higgs mass and are essentially generated via a stop-chargino loop. In the context of a CMSSM defined at M_{GUT} it is natural to ask what are the possible values of these masses and couplings $(m_A, \tan\beta, \dots)$ that can be reached consistently with all the phenomenological bounds.

We will analyze this problem discussing separately the case of $\mu > 0$ and $\mu < 0$. In fact $\text{sign}(\mu)$ is a key parameter in the analysis of the phenomenology of the large $\tan\beta$ limit for two main reasons. First, as well known and explained in detail in Sec. III, the sign of the SUSY

TABLE I. Numerical values of the SM input. Masses are given in GeV; for the leptons and the t quark the pole masses, for the lighter quarks the $\overline{MS}$ masses either at the mass scale itself, for c, b or for u, d, s, at the scale $Q = 2$ GeV. s_{ij} are the sines of the CKM mixing angle and δ the CKM phase.

m_e	$5.110 \ 10^{-4}$	m_t^{pole}	172.9
m_μ	0.1057	$m_b(m_b)$	4.25
m_τ	1.777	m_Z	91.1876
$m_u(Q)$	$3 \cdot 10^{-3}$	G_F	$1.1664 \cdot 10^{-5}$
$m_d(Q)$	$7 \cdot 10^{-3}$	$1/\alpha$	137.036
$m_s(Q)$	0.12	$\Delta \alpha_{\text{had}}^5$	0.02769
$m_c(m_c)$	1.2	$\alpha_s^{MS}(m_Z)$	0.1172
$s_{12} = 0.224$, $s_{23} = 4.13 \cdot 10^{-2}$, $s_{13} = 3.63 \cdot 10^{-3}$, $\delta = 1.13$			

TABLE II. Numerical values for the B-physics parameters using the notation of Ref. [10]. The lattice parameter has been taken from Ref. [89].

M_{Bs}	τ_{Bs}	η_B	$f_{Bs}\hat{B}_{Bs}^{1/2}$	$\tau(B_s)$	$\bar{P}_1^{LR}$	$\bar{P}_2^{LR}$	$\bar{P}_1^{SLL}$	$\bar{P}_2^{SLL}$
5.3696 GeV	1.461 ps	0.55	(294 ± 33) MeV	1.461 ps	-0.71	0.9	-0.37	-0.72

contributions to several low energy processes like $b \to s\gamma$ and the muon anomalous magnetic moment are determined by the sign of the μ parameter; therefore, the stringent experimental constraints tend to favor the positive sign of μ especially in the large $\tan\beta$ limit. In addition, as we have seen in Sec. II, the sign of the chargino one-loop corrections to the down quark Yukawa matrices and, in particular, of the ϵ_0 and $\tilde{\epsilon}_j$ parameters are also fixed by sign(μ). This implies that, in the basis of diagonal tree-level down Yukawa matrices, these one-loop corrections tend to reduce or increase these diagonal entries depending on the sign of μ and hence they give rise to a different phenomenology. In the $\mu > 0$ case, we have that both ϵ_0 and $\tilde{\epsilon}_j$ are positive; therefore, Eqs. (1)–(6) imply that the diagonal Higgs couplings to the down quarks are smaller than the naïve expectation, $\bar{m}_d/v_1$. As a consequence, for instance, FCNC couplings are smaller and effects of down quark Yukawa matrices in the RGE's are reduced.

The requirement of correct electroweak symmetry breaking sets an upper bound on $\tan\beta$. This is mainly a consequence of two difficulties: First, at large $\tan\beta$, both $m_{H_u}^2$ and $m_{H_d}^2$ become negative around the electroweak scale and the pseudoscalar Higgs becomes tachyonic, as can be seen in Fig. 3. Secondly, the bottom Yukawa becomes nonperturbative near the GUT scale. Furthermore, in the region with $M_0 \ll M_{1/2}$ there is the additional problem of the lighter stau becoming tachyonic. Therefore, the points of parameter space that succeed in generating a correct electroweak symmetry breaking with large $\tan\beta$ are strongly reduced. These problems are clearly softened if the entries in the down quark Yukawa matrices are small as it is the case with $\mu > 0$. In fact, for positive μ, values of $\tan\beta$ up to about 60 are still reachable in the CMSSM.

In the same way we must analyze the possible values of M_A. The mass of the pseudoscalar Higgs is approximately degenerate to the mass of the heavy scalar Higgs and both of them are related to the value of $|\mu|$. As already pointed out, at large values of $\tan\beta$ it is possible to reach smaller values of M_A due to the fact that $M_{H_d}^2$ gets negative which also is the reason for the smaller value of $|\mu|$. This can be seen in Fig. 3 where we show the possible values of M_A in the CMSSM as a function of $\tan\beta$ for fixed values of $M_{1/2} = 300$ GeV and $M_0 = 500$ GeV. As expected, we see the different behavior of M_A for positive or negative μ at large $\tan\beta$. For positive μ the value of M_A is larger than the corresponding value for negative μ and the same value of $\tan\beta$ due to the smaller effect of the down quark

Yukawas on the RGE running of m_{H_d}. In this plot, we do not include the experimental constraints on the SUSY parameter space from direct and indirect processes. In fact, making a general scanning of all the SUSY parameters, for $\mu > 0$, we can still find values of M_A as low as 150 GeV corresponding to $\tan\beta \gtrsim 50$ consistently with all constraints, see for instance Fig. 4.

Inserting $M_A = 150$ GeV, $\tan\beta = 60$, and $\mu > 0$ in the approximate formula given in Eq. (11) we obtain

$$\text{BR}(B_s \to \mu^+ \mu^-)$$
$$= 1.9 \times 10^{-4} \frac{A_t^2}{\mu^2} \frac{(H_2(m_{t_L}^2/\mu^2, m_{t_R}^2/\mu^2))^2}{(1 + \epsilon_0 \tan\beta)^2(1 + \tilde{\epsilon}_3 \tan\beta)^2}.$$
(46)

Taking $m_{\tilde{g}} \simeq \mu \simeq m_{\tilde{t}}$ and using $H_2(1, 1) \simeq -1/2$ we have $\epsilon_0 \simeq 0.012$ and $\tilde{\epsilon}_3 \simeq 0.015$. Therefore, a BR($B_s \to \mu^+ \mu^-$) between 10^{-7} and 5×10^{-6} would be the maximal value we can get in this model. In any case, we expect these regions of large $\tan\beta$ to be strongly constrained by other FCNC processes like $b \to s\gamma$ and δa_μ. In Figs. 4 and 5 we present the results for this branching ratio obtained using the complete formulas and taking into account all the
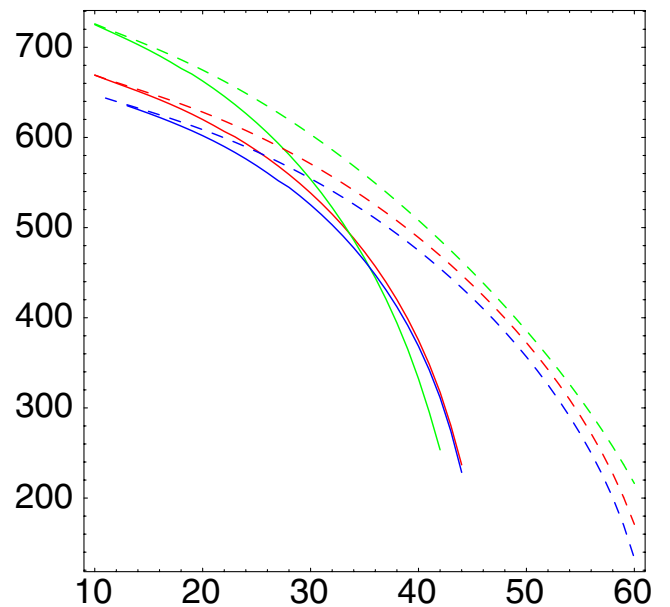

FIG. 3 (color online). Values of M_A as a function of $\tan\beta$ in the CMSSM. Full lines correspond to $\mu < 0$ and dashed lines to $\mu > 0$. The SUSY parameters are fixed as $m_{1/2} = 300$ GeV and $m_0 = 500$ GeV; the upper, central, and lower lines correspond to $A_0 = (0, -500, 500)$ GeV.
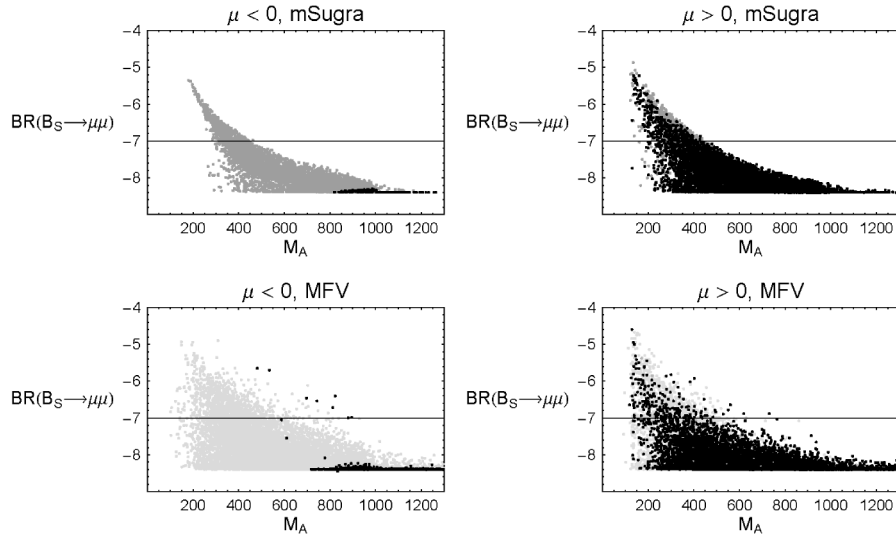
FIG. 4. Correlation between M_A and BR($B_s \to \mu^+ \mu^-$). All points satisfy the dark matter constraint. The gray points do not survive constraints from $B \to X_s \gamma$ and a_μ. Gray (orange) dots correspond to scenarios in which $C_7^{\text{eff}}(\mu_b) > 0$ although they do not satisfy the BR($b \to s l^+ l^-$) constraint.

constraints. Although many points that give rise to a large BR($B_s \to \mu^+ \mu^-$) are already excluded by the stringent bounds from FCNC processes, cancellations between different contributions in $b \to s\gamma$ still allow a large BR($B_s \to \mu^+ \mu^-$).

In Fig. 6 we compare the chargino and charged Higgs contributions to the Wilson coefficient $C_7(M_W)$ for the case of a BR($B_s \to \mu^+ \mu^-$) just below the current experimental bound. With positive μ, charged Higgs and chargino contributions tend to compensate and we can find many points in agreement with the $B \to X_s \gamma$ constraints. Moreover $M_{H^+}^2 \simeq M_A^2 + M_W^2$, thus a small pseudoscalar mass implies also a small charged Higgs mass. In fact, the experimentally allowed values for C_7^{tot} range from ~ -0.23 to ~ -0.08 while the contribution from the W boson is about

-0.17. This agrees with Fig. 6 where we can see that the chargino and charged Higgs contributions must be strongly correlated: in fact, their absolute value can be as large as 0.26 while their sum must range between -0.05 and $+0.10$. Therefore we see that, with positive μ, it is possible to have a light pseudoscalar and large $\tan\beta$ generating a large BR($B_s \to \mu\mu$) while at the same time keep the sum of chargino and charged Higgs contributions to $b \to s\gamma$ under control. Figure 6 also shows a couple of points for which the chargino contribution is sufficiently large to change the whole sign of the total Wilson coefficient at the low scale and still remain in agreement with experiments. From the discussion at the end of Sec. III B, it is clear that such points are excluded by the present measurement of BR($B \to X_s \ell^+ \ell^-$) because their contributions to
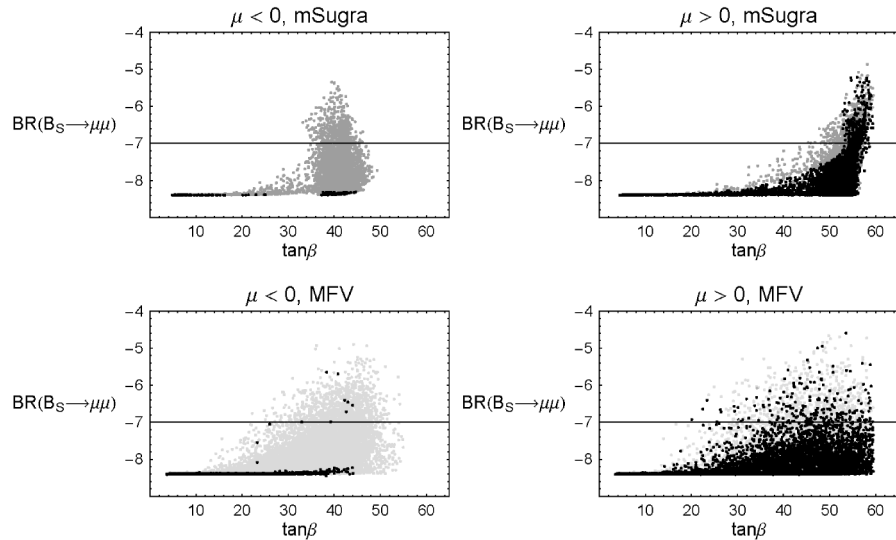

FIG. 5. BR($B_s \to \mu^+ \mu^-$) as a function of $\tan\beta$ in the CMSSM (upper plots) and MFV (lower plots). See the caption in Fig. 4.
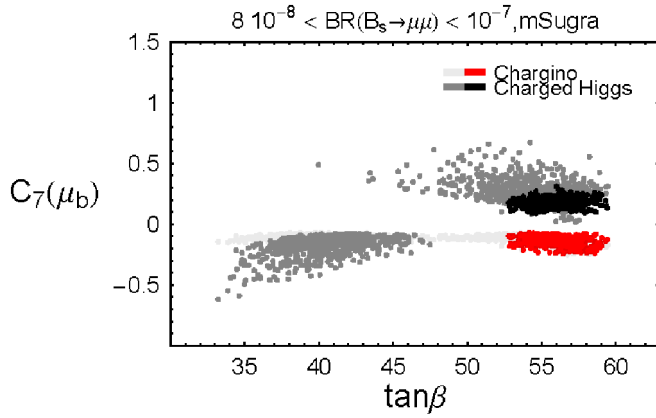
FIG. 6 (color online). Charged Higgs and chargino contributions to the C_7 Wilson coefficient in CMSSM as function of $\tan\beta$ corresponding to large BR($B_s \to \mu\mu$) and $\mu > 0$. Dark gray (red) points refer to chargino and black points to charged Higgs contributions. Light gray points do not survive the FCNC constraints.

C_9 and C_{10} (that lie within the black ellipsis drawn in Fig. 6) are too small.

A third process, closely related to the $B_s \to \mu\mu$ decay, is the $B_s - \bar{B}_s$ mass difference. As discussed in Sec. II, both processes involve the same FCNC neutral Higgs coupling, although they have a different M_A and $\tan\beta$ dependence. Note that in this case, the FCNC Higgs coupling enters twice as a double-penguin contribution and this implies that the change of sign(μ) does not affect the relative sign of the SUSY contribution to ΔM_{B_s} with respect to the SM one, that turns out to be always negative. However, the size of the FCNC Higgs couplings is smaller for $\mu > 0$ than for $\mu < 0$. Recently the D0 Collaboration was able to set for the first time an upper limit on ΔM_{B_s}: $\Delta M_{B_s} = (19 \pm 2)$ ps^{-1} at 90% C.L. [31]. It is necessary to

stress that this error is absolutely non-Gaussian and that there is a 5% probability that ΔM_{B_s} lies anywhere between 21 ps^{-1} and infinity. Shortly afterwards the CDF collaboration improved this bound [32]: $\Delta M_{B_s} = (17.33^{+0.42}_{-0.21}(\text{stat}) \pm 0.07(\text{syst}))$ ps^{-1}. Unfortunately this very precise experimental measure is not fully effective in constraining the SUSY parameter space due to the large uncertainty in the theoretical input parameters, mainly $f_{B_s}^2 B_{B_s}$ [90]. In Fig. 7 we compare ReM_{12}^s with BR($B_s \to \mu\mu$). In fact, $\Delta M_{B_s} = |M_{12}^s|$, but in our model, as in the SM, the phase of M_{12}^s is at the percent level and thus it is a very good approximation to the total ΔM_{B_s}. Moreover, plotting ReM_{12}^s allows us to control the change of sign of this amplitude. In this plot we fix the hadronic parameters to the values shown in Table II. As we can see in the second plot of Fig. 7 corresponding to $\mu > 0$, in the CMSSM and in the parameter space allowed by FCNC constrains it is not possible to change significantly the value of ΔM_{B_s} in the region with BR($B_s \to \mu^+\mu^-$) $\leq 10^{-6}$. Consequently no change of sign of ReM_{12}^s is possible in the CMSSM with $\mu > 0$. Given the present experimental bound on BR($B_s \to \mu^+\mu^-$) $\leq 10^{-7}$, we conclude that double-penguin contributions to ΔM_{B_s} cannot lower this mass difference below 17 ps^{-1}. To compare this value with the experimental measure by the CDF Collaboration we must take into account the uncertainty in the hadronic parameters. In Fig. 8 we present the range of values we can reach varying the value of $f_{B_s} B_{B_s}^{1/2}$ in the interval [0.259, 0.331] GeV [90]. As we can see, after taking into account the theoretical uncertainty, the ΔM_{B_s} constraint can never compete with the bound on BR($B_s \to \mu^+\mu^-$).

In the case of negative μ, we have that both ϵ_0 and $\tilde{\epsilon}_j$ are negative. Equations (1)–(6) imply that the diagonal Higgs couplings to the down quarks are larger than the naïve expectation, $\bar{m}_d/v_1$, and of the corresponding couplings
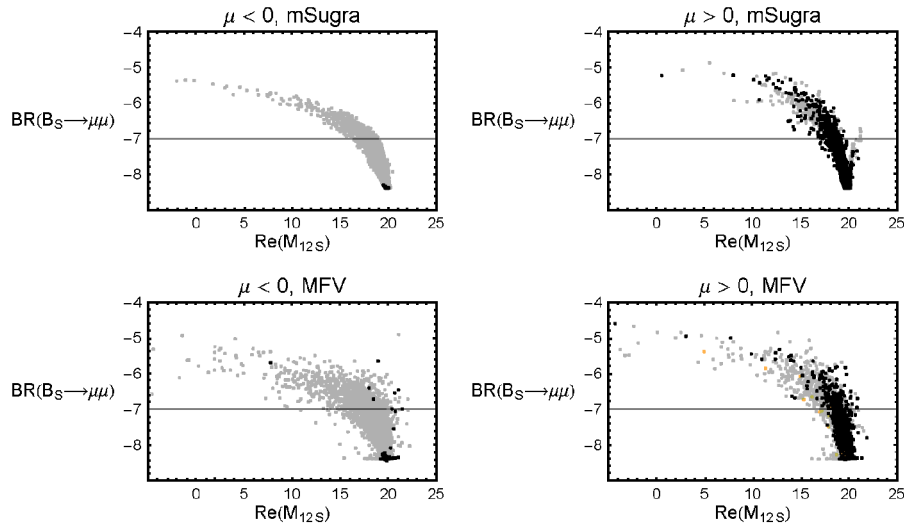

FIG. 7 (color online). Correlation between ReM_{12}^s and BR($B_s \to \mu^+\mu^-$). See the caption in Fig. 4.
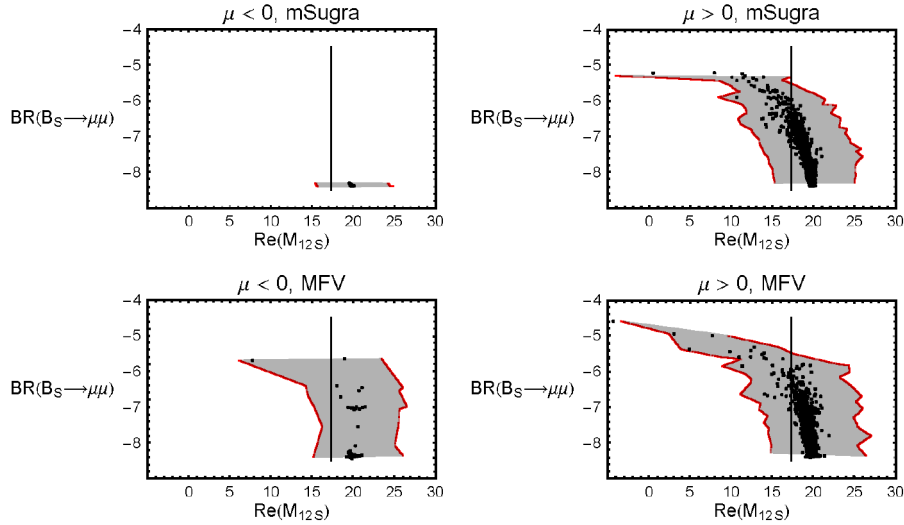
FIG. 8 (color online). Correlation between $\text{Re}M_{12}^s$ and $\text{BR}(B_s \to \mu^+\mu^-)$ including theory errors. The points satisfy all the constraints. The gray shaded area corresponds to theory uncertainties. The line is the experimental value of $\Delta M B_s$

for $\mu > 0$. Hence, FCNC couplings are larger and the effects of down quark Yukawa matrices in the RGE's is enhanced. This implies that the previously encountered problems with electroweak symmetry breaking occur now already at $\tan\beta \simeq 45$. Regarding the possible values of M_A, we see in Fig. 3 that, for negative μ, M_A tends to be much smaller than in the $\mu > 0$ case due to the effects of the large down quark Yukawas on m_{H_d}. Taking into account the constraints from $\text{BR}(B \to X_s \gamma)$ and a_μ, we can only find allowed points with $M_A \gtrsim 750 \, \text{GeV}$ and $\tan\beta \simeq 40$.

Taking $\mu < 0$, $x \simeq y \simeq 1$, and $m_{\tilde{g}} \simeq \mu \simeq m_{\tilde{l}}$ in Eq. (46), we get $\epsilon_0 \simeq -0.012$ and $\tilde{\epsilon}_3 \simeq -0.015$; thus, in principle, we obtain an extra enhancement from the denominator of Eq. (46) instead of the suppression we get in the case of $\mu > 0$. However, using the allowed masses (as obtained above) we find that the maximum branching ratio we can get is about $\simeq 10^{-7}$. In the numerical analysis, the maximum branching ratio we obtain is always below 10^{-8} as we can see in Fig. 5, because we have never obtained simultaneously these extreme values for the masses and the quantities ϵ_0, $\tilde{\epsilon}_j$ while being consistent with all the different constraints. In particular the $b \to s\gamma$ constraint requires heavy squarks and Higgs bosons and δa_μ requires in additions heavy sleptons. Therefore, the SUSY contributions to $\text{BR}(B_s \to \mu\mu)$ remain small for negative μ in the CMSSM.

Regarding the $B_s - \bar{B}_s$ mass difference, the double-penguin contribution has an opposite sign to the SM contribution, hence, reducing the predicted value of ΔM_{B_s}. As we explained above, Higgs FCNC couplings are now larger for $\mu < 0$ and we expect larger effects than for $\mu > 0$. In fact we see in Fig. 7 that with negative μ it is still possible to change the sign of $\text{Re}M_{12}^s$, although only very rarely. However, once we impose the indirect constraints we see that no change in ΔM_{B_s} from the SM expectations is

possible. This result seems to differ from the analogous plots (Fig. 23) of Ref. [9]. In fact, both figures would perfectly agree if the $b \to s\gamma$ constraints are not imposed. This is only due to the difference in the MSSM models considered in both works. Buras *et al.* analyze a general MSSM defined at the electroweak scale with the different parameters unrelated and only constrained by low energy experimental observables. In this framework they have the freedom to assume a relative sign between A_t and μ independently of the sign of μ. In our model, all the parameters are defined at M_{GUT} and the sign of A_i at the electroweak scale is always negative due to the dominant (negative) gaugino contribution in the RGE evolution. Therefore our results would agree without the $b \to s\gamma$ and δa_μ constraints: taking into account these constraints, large effects are not possible in this GUT inspired model.

Finally, we analyze the effect of dark matter constraints on this process. Although the lightest neutralino of the CMSSM is a good dark matter candidate, it is well known that in most of the parameter space of this model a too large dark matter density is generated. Only under certain specific conditions a correct value of $\Omega_{\tilde{\chi}^0} h^2$ is generated after annihilation of the excess neutralinos among themselves or coannihilation with other light sparticles. The regions where these conditions are possible follow:

(1) The bulk annihilation region, at low values of $m_{1/2}$ and m_0, where neutralinos annihilate in pairs at a sufficient rate via t-channel slepton exchange.

(2) The stau coannihilation region, where neutralinos coannihilate with staus, given that $m_{\tilde{\chi}^0} \simeq m_{\tilde{\tau}}$.

(3) The focus point region, at large m_0 where the value of $|\mu|$ is small and the neutralinos have a significant Higgsino component enhancing the annihilation into WW and ZZ pairs.

(4) The funnel region, which occurs at very large $\tan\beta \sim 45$–60 and the pseudoscalar mass $m_A \sim 2m_{\tilde{\chi}^0}$ so that
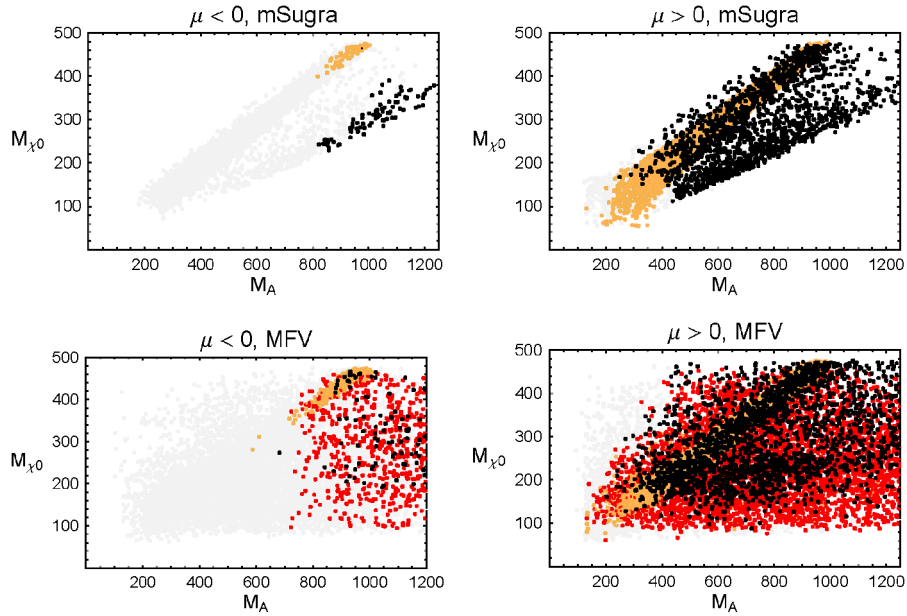
FIG. 9 (color online).   Correlation between M_A and $M_{\tilde{\chi}^0}$. Black and light gray (orange) points corresponds to stau coannihilation and funnel, respectively. In the MFV case, the dark matter constraint also can be fulfilled by a neutralino with a sizeable Higgsino component [dark gray (red) points].

neutralinos annihilate into a fermion pair through a pseudoscalar Higgs boson in the s channel.

Given that in this paper we are mainly interested in the large $\tan\beta$ region, it is clear that we can expect the funnel region to play a special role in our analysis. In Figs. 9 and 10 we plot the allowed points in the $m_A - m_{\tilde{\chi}^0}$ and $m_{\tilde{\tau}} - m_{\tilde{\chi}^0}$ planes. Here we select points in the stau coannihilation region (black points) for which the difference between $m_{\tilde{\tau}}$ and $m_{\tilde{\chi}^0}$ is less than 10%. Similarly we select the funnel points when $(M_A - 2m_{\tilde{\chi}^0})/\Gamma_A \leq 6$. Taking into account

that $\Gamma_A \propto M_A \tan^2\beta(3m_b^2 + m_\tau^2)$, we have that at large $\tan\beta$ the difference between neutralino and pseudoscalar masses can be larger. In Fig. 9, we see that the funnel region is wider at low pseudoscalar masses because low pseudoscalar masses correspond to large $\tan\beta$. In the same way, Fig. 10 shows clearly all the coannihilation points concentrated around the $M_A \simeq 2m_{\tilde{\chi}^0}$ line. It is interesting to notice that we have points where both the funnel and coannihilation mechanisms are active (although we plot them as coannihilation points, i.e. black points). In fact, in
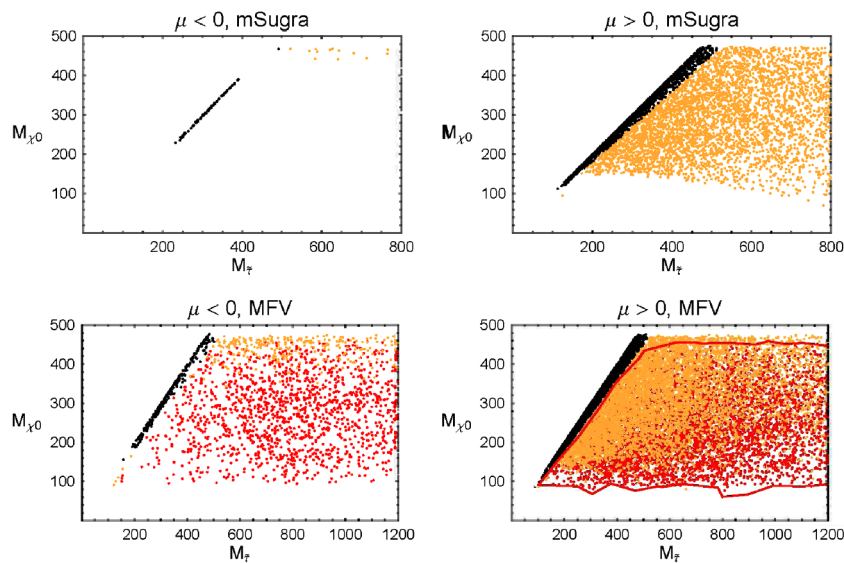

FIG. 10 (color online).   Correlation between $M_{\tilde{\tau}}$ and $M_{\tilde{\chi}^0}$. See the caption in Fig. 9.

these points the cross sections for $\tilde{\chi}^0 \tilde{\tau}_1^+ \to \gamma \tau^+$ and/or $\tilde{\tau}_1^+ \tilde{\tau}_1^- \to f\bar{f}$ constitute more than 10% of the total annihilation of SUSY particles. This means that these points correspond to the coannihilation region. Moreover the ratio of $\tilde{\chi}^0 \tilde{\chi}^0 \to b\bar{b}$ and $\tilde{\chi}^0 \tilde{\chi}^0 \to \tau^+ \tau^-$ channels is proportional to $(m_b/m_\tau)^2$ which means they are mediated by a Higgs particle and hence they belong also to the funnel region.

In the CMSSM we scan values of m_0 and $M_{1/2}$ up to 1 TeV and thus we do not enter the focus point region. In any case, points belonging to the focus point region have very heavy sfermion and pseudoscalar Higgs masses and therefore they have no effect on the processes we are analyzing here. The bulk region is already very constrained in the CMSSM scenario due to the bounds on the masses of the lighter chargino and the light scalar Higgs boson and pure bulk annihilation is nearly excluded.

In Fig. 11 we present for completeness the correlation between M_A and $M_{\tilde{\chi}^0}$ imposing the full one-sigma bound on the dark matter abundance from Eq. (44). In this case the number of allowed points is reduced but the main features of our analysis remain valid.

C. $B_s \to \mu^+ \mu^-$ in the general MFV MSSM

In this section we analyze the effects of flavor-changing Higgs couplings in a general MFV MSSM defined at the GUT scale. In this model we assign different soft masses and trilinear couplings to the different representations under the SM gauge group and thus we have 13 independent parameters. The main difference with the CMSSM analyzed in the previous section concerns precisely the Higgs soft masses that are not related with the squark or slepton masses. In this way we can obtain lighter Higgs masses while at the same time the sfermion masses are heavy enough to satisfy the stringent FCNC constraints.

Again we distinguish the cases of $\mu > 0$ and $\mu < 0$. Analogously to the CMSSM case, $\mu > 0$ implies that both ϵ_0 and $\bar{\epsilon}_j$ are negative. Therefore Yukawa couplings are reduced and their effects in FCNC and the RGE evolution is smaller.

The values that can be obtained for m_A and $\tan\beta$ in this general MFV model are similar to the values obtained in the CMSSM case, as can be seen in Fig. 12. Therefore, in principle, similar values for the BR($B_s \to \mu^+ \mu^-$) are
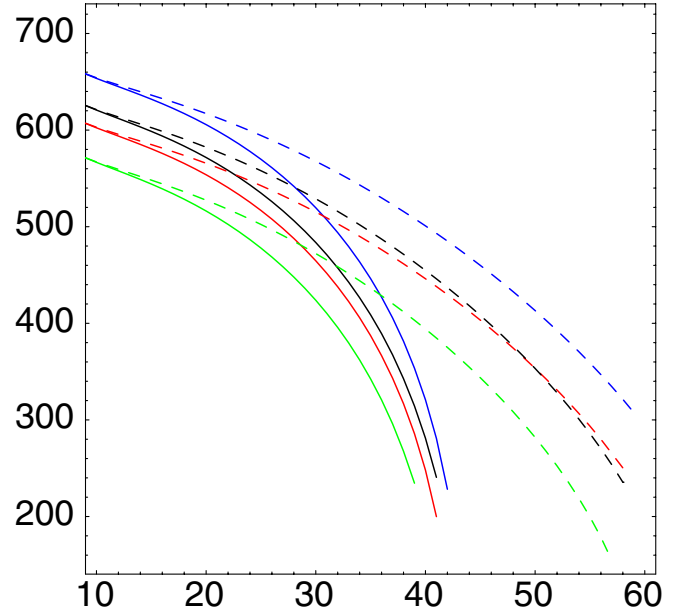

FIG. 12 (color online). Values of m_A as a function of $\tan\beta$ in the CMSSM. In this plot all sfermion masses are equal to 500 GeV and $m_{1/2} = 300$ GeV and $A_0 = 0$. Full lines correspond to $\mu < 0$ and dashed lines to $\mu > 0$. Starting from the uppermost line downward, the Higgs mass parameters are $m_{H_1}, m_{H_2} = \{(300, 150), (300, 300), (150, 150), (150, 300)\}$ GeV, respectively.

possible in both models. However, as we will show here, after taking into account the FCNC constraints, combinations of $(m_A, \tan\beta)$ that would be forbidden in the CMSSM are now allowed in the MFV model. Thus it is easier to obtain larger values for BR($B_s \to \mu^+ \mu^-$) consistently with the FCNC constraints. This can be seen in Figs. 4 and 5 where for positive μ we obtain similar values for BR($B_s \to \mu^+ \mu^-$) as in the CMSSM case although the dependence of BR($B_s \to \mu^+ \mu^-$) on M_A and $\tan\beta$ is less defined than in the CMSSM case. In these figures we find larger values for the branching ratios with respect to the CMSSM case with smaller values of M_A or $\tan\beta$.

How are the $b \to s\gamma$ and a_μ constraints satisfied in this case? The main difference between the CMSSM and the MFV model is the fact that now different scalar masses are independent and therefore it is possible to have light Higgs
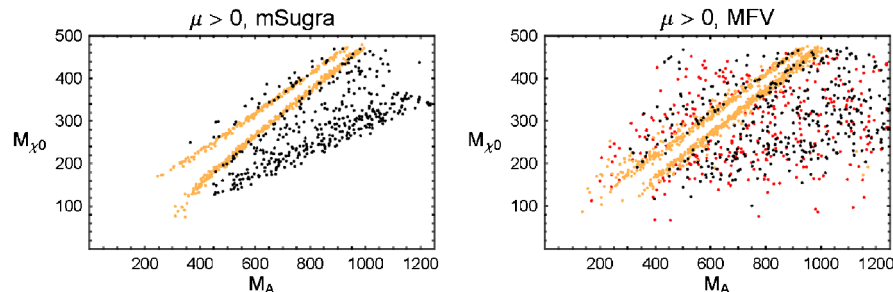

FIG. 11 (color online). Impact of the one-sigma dark matter bound on the correlation between M_A and $M_{\tilde{\chi}^0}$.

masses with heavy sfermions. Apart from this difference, the case of positive μ is qualitatively similar to the CMSSM. In Fig. 13 we present the values of the Wilson coefficients C_7^H and $C_7^{\tilde{\chi}}$ for $\mu > 0$ and $\mu < 0$. For $\mu > 0$ the situation is very similar to the situation we found in the CMSSM. The only difference is that we can find points with $\mathrm{BR}(B_s \to \mu^+ \mu^-) > 5 \times 10^{-8}$ for comparatively smaller values of $\tan\beta$ and that we do find several points with $C_7^{\tilde{\chi}} > 1$ that change the total sign of C_7, although they are always forbidden by the $B \to X_s l^+ l^-$ constraint as expected [51].

Regarding the $B_s - \bar{B}_s$ mass difference, we see in Fig. 7 that for $\mu > 0$, the MFV case is still very similar to the CMSSM one. However we can see that now it is possible to change the sign of $\mathrm{Re}(M_{12}^s)$ if we disregard the $(B_s \to \mu^+ \mu^-)$ constraint. Once we impose the new CDF and D0 constraint on $\mathrm{BR}(B_s \to \mu^+ \mu^-)$, no sizeable change in ΔM_{B_s} is possible and taking into account the theoretical errors as done in Fig. 8 the allowed points always agree with the recent experimental result from the CDF collaboration.

In all these plots, the main difference between the CMSSM and the MFV cases can be seen for $\mu < 0$. Once more $\mu < 0$ implies that both ϵ_0 and ϵ_j are negative. From Figs. 4 and 5 we can see that, as opposed to the CMSSM case, we can reach $\mathrm{BR}(B_s \to \mu^+ \mu_-) \simeq 10^{-6}$ with $\mu < 0$ consistently with all the constraints and for values of $\tan\beta$ as low as 40. This is due to the negative sign of the parameters ϵ_0 and $\tilde{\epsilon}_3$. In fact for $\mu > 0$ the factor $1/((1 + \epsilon_0 \tan\beta)(1 + \tilde{\epsilon}_3 \tan\beta))$ can amount to a suppression by a factor 10 for $\tan\beta = 50$ and $\epsilon_0 = 0.012$ while it represents an enhancement factor of 20 for $\tan\beta = 40$ and $\epsilon_0 = -0.012$. Therefore, for the same values of M_A and $\tan\beta$ we can get an enhancement of 2 orders of magnitude when changing from $\mu > 0$ to $\mu < 0$.

The main question is how are the different indirect constraints satisfied for these points. From Fig. 13, we see that, in this case, both C_7^H and $C_7^{\tilde{\chi}}$ are negative as expected and both of them are very small as required by the $b \to s\gamma$ constraint summing up to, at most, 0.05. This is possible only with a rather heavy spectrum although we

want to keep the Higgses as light as possible in order to have a large $\mathrm{BR}(B_s \to \mu^+ \mu^-)$. Similarly, even taking a conservative a_μ bound at 3σ, only a rather heavy SUSY spectrum is allowed. However, in this model the Higgs masses are independent from the rest of the SUSY spectrum and hence we can still find sizable Higgs contributions to the decay $(B_s \to \mu^+ \mu^-)$. In any case it is clear from the density of point with large branching ratio that all these points require a certain degree of fine-tuning to satisfy these requirements.

Finally we discuss the dark matter constraints. From Figs. 9 and 10 we can see the regions of parameter space allowed by the dark matter constraints. The main difference between the CMSSM case and the general MFV scenario is the appearance of a new set of allowed points that correspond to neutralinos with a sizeable Higgsino component. This also has been noted previously in models where the Higgs-mass parameter has been decoupled from the sfermion parameters [23–25]. Now the coupling of the Z boson to a lightest supersymmetric particle pair is enhanced and the neutralinos annihilate through a Z boson in the s channel. This situation is similar to the focus point region in the CMSSM. However, in contrast to the focus point situation, the sfermions and Higgs masses can be still of the order of a few hundred GeVs. This leads to the observed smear-out of the different regions in the MFV scenario.

V. LARGE $\mathrm{BR}(B_s \to \mu^+ \mu^-)$ COLLIDER PHENOMENOLOGY

In the first part of this section we assume that a branching ratio for the decay $B_s \to \mu^+ \mu^-$ has been measured between 8×10^{-8} and 10^{-7} and explore the consequences for the phenomenology of high energy colliders [91]. In the second part we will briefly comment on the occurrence of flavor violating SUSY decays.

We have seen in the previous section, that such a large branching ratio for $B_s \to \mu^+ \mu^-$ requires a light pseudo-scalar Higgs boson and large $\tan\beta$ as it scales as $\tan^6\beta/m_{A^0}^4$. In the case of the CMSSM this indeed implies
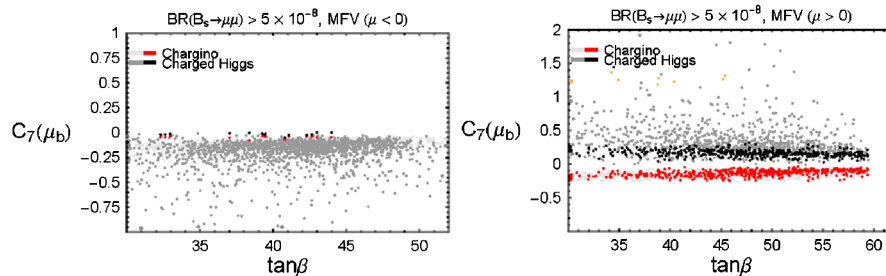

FIG. 13 (color online). Charged Higgs and chargino contributions to the C_7 Wilson coefficient in MFV as a function of $\tan\beta$. Dark gray (red) points refer to chargino and black points to charged Higgs contributions. Gray (orange) points are points where C_7^{tot} changes sign although they are not allowed by the $\mathrm{BR}(b \to s l^+ l^-)$ constraint. Gray points do not survive the FCNC constraints.
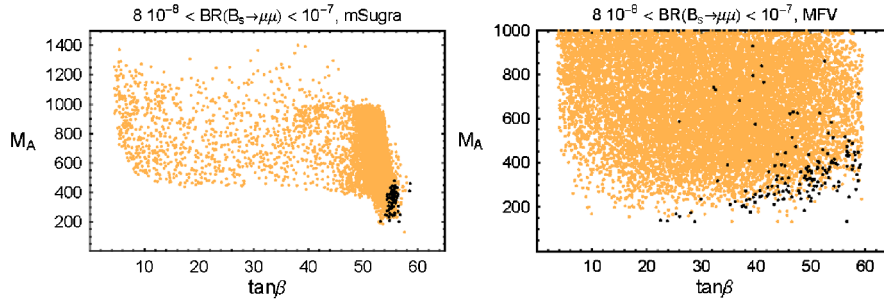
FIG. 14 (color online). Correlation between $\tan\beta$ and M_A in a large $B_s \rightarrow \mu\mu$ scenario. Gray (orange) points have $BR(B_s \rightarrow \mu\mu) < 8 \times 10^{-8}$; black points have $8 \times 10^{-8} < BR(B_s \rightarrow \mu\mu) < 10^{-7}$.

an upper bound of about 570 GeV and a low bound on $\tan\beta$ of about 50 as can be seen in the left plot of Fig. 14 where the black points are those satisfying all low energy bounds while yielding the large branching ratio. In the right plot of Fig. 14 we see that these bounds get considerably weaker in the MFV case. The reason is that the tight correlations between the various SUSY masses is broken up and it is easier to satisfy the low energy constraints, in particular $b \rightarrow s\gamma$. Nevertheless, we find a lower bound of about 20 for $\tan\beta$ and an upper one of about 950 GeV for m_{A^0}. In the CMSSM upper bounds on the masses of other particles are obtained, e.g. the chargino has to be lighter than 600 GeV as can be seen from Fig. 15 where $m_{\tilde{\chi}_1^+}$ is shown versus $m_{\tilde{t}_1}$. In the case of the MFV scenario the bound on $m_{\tilde{\chi}_1^+}$ is about 850 GeV. Note that the upper bound on $m_{\tilde{\chi}_1^+}$ implies in CMSSM (MFV) also an upper bound on $m_{\tilde{g}}$ of about 1.7 TeV (2.4 TeV). As a consequence the discovery of SUSY [92] is guaranteed in both scenarios due to gluino production. An important question is if the heavier Higgs boson can be detected at LHC. In the CMSSM it turns out that in the region with large $BR(B_s \rightarrow \mu^+\mu^-)$ the heavier neutral Higgs bosons can be detected via the decays into the $\tau^+\tau^-$ final state with 30 fb^{-1}; see [93] and references therein. In the region with $M_{A0} \lesssim 350$ GeV also the $\mu^+\mu^-$ final state can be used in case of an integrated luminosity of 60 fb^{-1}. Also the charged Higgs bosons should be visible via its decay into $\tau\nu_\tau$ [93]. In the case of the general MFV scenarios the regions with $\tan\beta \lesssim 25$

and/or $m_{A0} \gtrsim 800$ GeV will most likely require larger statistics for detecting the heavy Higgs bosons. In the MFV scenario and to a much lesser extent in the CMSSM scenario there are some points with $m_{H^+} < m_t - m_b$ implying that the branching ratio $t \rightarrow b\tau^+\nu_\tau$ will be modified. Numerically we find that there are 3 (10) data points (out of 40 000 points) in the region with $BR(B_s \rightarrow \mu^+\mu^- > 8 \cdot 10^{-8})$ [$BR(B_s \rightarrow \mu^+\mu^- < 8 \cdot 10^{-8})$] with a maximal value of $BR(t \rightarrow b\tau^+\nu_\tau)$ of 12 (21)%.

We also have checked if the running from M_{GUT} down to M_{EWSB} can induce any sizable flavor violating branching ratio in the decays of SUSY particles. As expected, these decay branching ratios are in general very small, of the order 10^{-5} and below. There are a few points in the MFV scenario where BRs of the order 10^{-3} can be obtained e.g. for $\tilde{b}_1 \rightarrow \tilde{\chi}_1^- c$ due to a kinematical suppression of $\tilde{b}_1 \rightarrow \tilde{\chi}_1^- t$ and $\tilde{b}_1 \rightarrow \tilde{\chi}_2^0 b$. In these points $\tilde{b}_1$ is mainly a $\tilde{b}_L$ and thus the coupling $\tilde{b}_1 - \tilde{\chi}_1^0 - b$ is reduced due to the small hypercharge of $\tilde{Q}_L$ implying a reduction in the decay mode $\tilde{b}_1 \rightarrow \tilde{\chi}_1^0 b$. However, it has to be expected that the SUSY background of $\tilde{s}_L \rightarrow \tilde{\chi}_1^- c$ will be too large to observe this mode at LHC.

In the literature (for an incomplete list see [94–107]) often an approximate solution of the $\tilde{t}_1 - c - \tilde{\chi}_1^0$ coupling is used which results from a one-loop integration of the flavor violating RGEs for $M_{Q,23}^2$ and $A_{u,23}$ [108] resulting in a mixing between $\tilde{c}_L$ and $\tilde{t}_1$. The projection ϵ of $\tilde{c}_L$ onto $\tilde{t}_1$ can be written as:
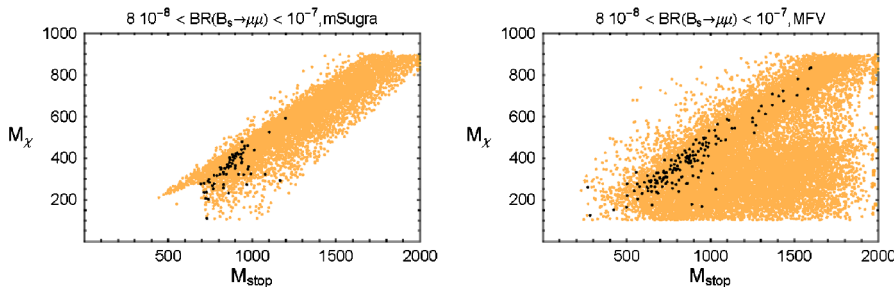

FIG. 15 (color online). Correlation between $M_{\tilde{t}}$ and $M_{\tilde{\chi}^\pm}$ in a large $B_s \rightarrow \mu\mu$ scenario. Gray (orange) points have $BR(B_s \rightarrow \mu\mu) < 8 \times 10^{-8}$; black points have $8 \times 10^{-8} < BR(B_s \rightarrow \mu\mu) < 10^{-7}$.

$$\epsilon = \frac{\Delta_L \cos\theta_t + \Delta_R \sin\theta_t}{m_{\tilde{c}_L}^2 - m_{\tilde{t}_1}^2}, \tag{47}$$

$$\Delta_L = -\frac{g^2}{16\pi^2} \ln\left(\frac{M_X^2}{m_W^2}\right) V_{tb}^* K_{cb} Y_b^2 (M_{\tilde{Q},3}^2 + M_{\tilde{d}_R,3}^2 + M_{H_1}^2 + A_b^2), \tag{48}$$

$$\Delta_R = \frac{g^2}{16\pi^2} \ln\left(\frac{M_X^2}{m_W^2}\right) V_{tb}^* K_{cb} Y_b^2 m_t A_b, \tag{49}$$

resulting in the $\tilde{t}_1 - c - \tilde{\chi}_1^0$ interaction

$$\mathcal{L} = -\sqrt{2}\left(\frac{g' N_{11}}{6} + \frac{g N_{12}}{2}\right)\epsilon \bar{c} P_R \tilde{\chi}_1 \tilde{t}_1 + \text{H.c.} \tag{50}$$

Here θ_t is the mixing angle between left and right stops. All the quantities should be taken at the M_{GUT} as this is a one-step integration of the RGES. Because of the largeness of m_t it can happen that all two-body decays of $\tilde{t}_1$ are kinematically suppressed or even forbidden at tree-level and that the main decay mode is $\tilde{t}_1 \rightarrow \tilde{\chi}_1^0 c$. In the MFV scenario we find indeed a couple of points where the tree-level decays are suppressed. These are the points shown in the lower left corner of Fig. 15. Depending on the coupling strength it might be possible that $\tilde{t}_1$ hadronizes before decaying and therefore it is important to check the quality of this approximation. In Fig. 16 we show the ratio of the approximate coupling over the exact calculation using numerical solutions of the RGEs. One sees that for nonzero A_0 the approximation gives roughly the order of magnitude but can be by a factor 100 in certain cases. Note that this corresponds to a factor 10^4 in the partial width. In the case $A_0 = 0$ the difference can even be larger which is due to the smallness of the exact coupling. The minimum of the exact coupling around $\tan\beta = 10$ is due to a cancellation between the $\tilde{t}_L - \tilde{c}_L$ mixing and the $\tilde{t}_R - \tilde{c}_L$ which is not obtained within the approximation because the $\tilde{t}_R - \tilde{c}_L$ is zero in this case. We have used the approximation formula

for the calculation of the decay $\tilde{t}_1 \rightarrow c\tilde{\chi}_1^0$ getting a maximal branching ratio of $7 \cdot 10^{-3}$ which is about a factor of 200 larger than the exact calculation. From this we conclude that results obtained using this approximate formula have to be taken with some care and that an observation of the decay mode $\tilde{t}_1 \rightarrow c\tilde{\chi}_1^0$ would be a clear indication of the existence of nonminimal flavor violation structures.

VI. CONCLUSIONS

We have analyzed flavor-changing processes in a minimal flavor violating supersymmetric model at the GUT scale. Two examples of this kind have been studied and compared in more detail; the usual constrained MSSM and a completely generic MFV model defined at the GUT scale. In the analyses of these models we have used two-loop renormalization group equations taking into account for the first time the complete flavor structure in the running of the parameters. We have applied all the updated constraints available at the moment including the last measurement of the B_s mass difference by CDF and the dark matter relic abundance from the third year results of the WMAP experiment.

The main objective of our analysis has been the study of the $B_s \rightarrow \mu^+\mu^-$ decay. This decay rate is enhanced by additional powers of $\tan\beta$ when mediated by neutral Higgses. In both the generic MFV and even the CMSSM scenario we indeed find that enhancements of the BR($B_s \rightarrow \mu^+\mu^-$) of several orders of magnitude are still possible consistently with all other constraints. This implies that the present bound from the D0 and CDF experiments already can rule out a large part of large $\tan\beta$ and small M_A regions in the parameter space of these models.

In the CMSSM, large values (close to the current bound) for the $B_s \rightarrow \mu^+\mu^-$ decay would necessarily imply a value of $\tan\beta \gtrsim 50$, a light pseudoscalar, $M_A \lesssim 570$ GeV, and positive sign of the μ parameter. These points of the parameter space can still satisfy the stringent
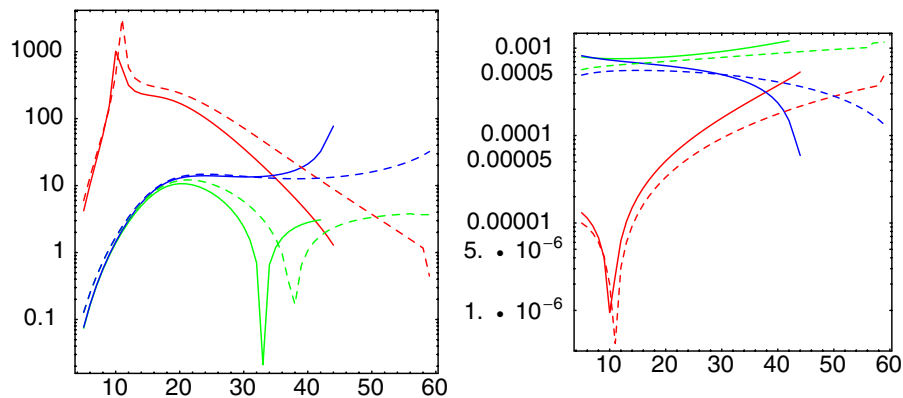

FIG. 16 (color online). Left plot: approximate $\tilde{t}_1 - c - \tilde{\chi}_1^0$ coupling over the exact one as a function of $\tan\beta$ in the CMSSM. Right plot: exact $\tilde{t}_1 - c - \tilde{\chi}_1^0$ couplings a function of $\tan\beta$ in the CMSSM. In both plots, full lines correspond to $\mu < 0$ and dashed lines to $\mu > 0$. The SUSY parameters are fixed as $m_{1/2} = 300$ GeV, $m_0 = 500$ GeV. Starting from the uppermost line downward, we have $A_0 = (-500, 500, 0)$ GeV in the left plot and $A_0 = (0, 500, -500)$ GeV in the right plot.

$b \to s\gamma$ constraints due to the opposite sign of the chargino and charged Higgs contributions. We have also checked explicitly that the new constraint from $\mathrm{BR}(B \to X_s l^+ l^-)$ eliminate all the points of the parameter space where a large chargino contribution is able to reverse the sign of the C_7 Wilson coefficient. Unfortunately, the new experimental results on the B_s mass difference are not effective to constrain the parameter space of the CMSSM once the $B_s \to \mu^+ \mu^-$ bounds are applied. This is due to the large theoretical uncertainty in the calculation of the B_s mass difference. With respect to the dark matter constraints, we have seen that the allowed points with sizeable flavor-changing effects correspond to the funnel and coannihilation regions.

In the generic MFV model, many of the well-defined regions observed in the CMSSM scenario are smeared out due to the fact that the Higgs masses are now independent from the other soft-breaking parameters. Now, having $8 \times 10^{-8} \leq \mathrm{BR}(B_s \to \mu^+ \mu^-) \leq 1 \times 10^{-7}$ would only require $\tan\beta \gtrsim 20$ and $M_A \lesssim 950$ GeV. Moreover, it is still possible to obtain these large branching ratios with negative values of the μ parameter at the expense of some fine-tuning to fulfil the $b \to s\gamma$ constraint and satisfy the δa_μ bound at the 3σ level. As in the CMSSM case, the lack of more precise hadronic parameters in B_s decays prevents us to use the precise experimental results to further constrain the allowed parameter space. Furthermore we have seen that in a generic MFV scenario at the GUT scale a new set of points with a correct dark matter abundance appears, corresponding to neutralinos with a large Higgsino component. These points can still have relatively light Higgses and sfermions compared to the focus point region of the CMSSM, and therefore their contribution to FCNC processes can be sizeable.

Finally, we also have explored the phenomenology to be expected at collider experiments as LHC if a $8 \times 10^{-8} \leq \mathrm{BR}(B_s \to \mu^+ \mu^-) \leq 1 \times 10^{-7}$ is measured. The main feature of this scenario is that the SUSY spectrum is relatively light and SUSY should be discovered at LHC. The neutral and charged Higgses in this scenario should also be visible at the LHC. In some cases with light m_{H^+} the branching ratio of the top quark into $b\tau^+\nu_\tau$ will be modified from the SM expectations due to charged Higgs mediation. We have studied the flavor violating decay $t \to \chi_1^0 c$ and we have found that large branching ratios are not found in contrast with the results in the literature obtained using approximate formulas.

APPENDIX A: SFERMION MASS MATRIX

The 6×6 sfermion mass matrices are given by

$$M_{\tilde{f}}^2 = \begin{pmatrix} M_{\tilde{f}_L}^2 + (T_I^3 - Q_f \sin^2\theta_W)\cos 2\beta m_Z^2 + M_f^2 & Y_{A_f}^* \frac{v}{\sqrt{2}}\Omega(\beta) - M_f \mu\Theta(\beta) \\ Y_{A_f}\frac{v}{\sqrt{2}}\Omega(\beta) - M_f \mu^*\Theta(\beta) & M_{\tilde{f}_R}^2 + Q_f \sin^2\theta_W \cos 2\beta m_Z^2 + M_f^2 \end{pmatrix}, \quad (A1)$$

where

$$\begin{cases} \Theta(\beta) = \cot\beta, \Omega(\beta) = \sin\beta & \text{for } T_I^3 = \frac{1}{2} \\ \Theta(\beta) = \tan\beta, \Omega(\beta) = \cos\beta & \text{for } T_I^3 = -\frac{1}{2} \end{cases}, \quad (A2)$$

and Y_{A_f} are the trilinear matrices equal at M_{GUT} to $Y_{A_f} = Y_f A_f$. These matrices are diagonalized by the 6×6 unitary matrices Γ_f:

$$\mathrm{diag}\,(M_{\tilde{f}_1}, \ldots, M_{\tilde{f}_6}) = \Gamma_{\tilde{f}} \cdot M_{\tilde{f}}^2 \cdot \Gamma_{\tilde{f}}^\dagger. \quad (A3)$$

The 6×3 left and right block components of the mixing matrices are defined as

$$\Gamma_{\tilde{f}}^{6\times 6} = (\Gamma_{\tilde{f}L}^{6\times 3} \Gamma_{\tilde{f}R}^{6\times 3}). \quad (A4)$$

In the flavor-blind scenario, the most important off-diagonal entry in the above squared mass matrices is the third generation LR mixing. Below we present the analytic expressions of the 2×2 stop system:

$$M_{\tilde{t}}^2 = \begin{pmatrix} M_{\tilde{t}_{LL}}^2 & e^{-i\varphi_{\tilde{t}}} M_{\tilde{t}_{LR}}^2 \\ e^{i\varphi_{\tilde{t}}} M_{\tilde{t}_{LR}}^2 & M_{\tilde{t}_{RR}}^2 \end{pmatrix}, \quad (A5)$$

where

$$M_{\tilde{t}_{LL}}^2 = m_{Q_3}^2 + (\tfrac{1}{2} - \tfrac{2}{3}\sin^2\theta_W)\cos 2\beta m_Z^2 + m_t^2, \quad (A6)$$

$$M_{\tilde{t}_{RR}}^2 = m_{U_3}^2 + \tfrac{2}{3}\sin^2\theta_W \cos 2\beta m_Z^2 + m_t^2, \quad (A7)$$

$$M_{\tilde{t}_{LR}}^2 = m_t |A_t - \mu^*\Theta(\beta)|, \quad (A8)$$

$$\varphi_{\tilde{t}} = \arg[A_t - \mu^* \Theta(\beta)]. \tag{A9}$$

The eigenvalues are given by

$$2m^2_{\tilde{t}_1, \tilde{t}_2} = (M^2_{\tilde{t}_{LL}} + M^2_{\tilde{t}_{RR}}) \mp \sqrt{(M^2_{\tilde{t}_{LL}} - M^2_{\tilde{t}_{RR}})^2 + 4(M^2_{\tilde{t}_{LR}})^2}, \tag{A10}$$

with $m^2_{\tilde{t}_1} \le m^2_{\tilde{t}_2}$. We parametrize the mixing matrix $\mathcal{R}^{\tilde{t}}$ so that

$$\begin{pmatrix} \tilde{t}_1 \\ \tilde{t}_2 \end{pmatrix} = \mathcal{R}^{\tilde{t}} \begin{pmatrix} \tilde{t}_L \\ \tilde{t}_R \end{pmatrix}$$

$$= \begin{pmatrix} e^{(i/2)\varphi_{\tilde{t}}} \cos\theta_{\tilde{t}} & e^{-(i/2)\varphi_{\tilde{t}}} \sin\theta_{\tilde{t}} \\ -e^{(i/2)\varphi_{\tilde{t}}} \sin\theta_{\tilde{t}} & e^{-(i/2)\varphi_{\tilde{t}}} \cos\theta_{\tilde{t}} \end{pmatrix} \begin{pmatrix} \tilde{t}_L \\ \tilde{t}_R \end{pmatrix}, \tag{A11}$$

where $\varphi_{\tilde{t}}$ is given in Eq. (A9) and

$$\cos\theta_{\tilde{t}} = \frac{-M^2_{\tilde{t}_{LR}}}{\Delta} \le 0, \qquad \sin\theta_{\tilde{t}} = \frac{M^2_{\tilde{t}_{LL}} - m^2_{\tilde{t}_1}}{\Delta} \ge 0,$$

$$\Delta^2 = (M^2_{\tilde{t}_{LR}})^2 + (m^2_{\tilde{t}_1} - M^2_{\tilde{t}_{LL}})^2. \tag{A12}$$

APPENDIX B: CHARGINO MASS MATRIX

The chargino mass matrix

$$M^{\tilde{\chi}^+}_{\alpha\beta} = \begin{pmatrix} M_2 & m_W \sqrt{2} \sin\beta \\ m_W \sqrt{2} \cos\beta & \mu \end{pmatrix} \tag{B1}$$

can be diagonalized by the biunitary transformation

$$U^*_{j\alpha} M^{\tilde{\chi}^+}_{\alpha\beta} V^*_{k\beta} = m_{\tilde{\chi}^+_j} \delta_{jk}, \tag{B2}$$

where U and V are unitary matrices such that $m_{\tilde{\chi}^+_j}$ are positive and $m_{\tilde{\chi}^+_1} < m_{\tilde{\chi}^+_2}$.

APPENDIX C: NEUTRALINO MASS MATRIX

We define $N_{\alpha j}$ as the unitary matrix which makes the complex symmetric neutralino mass matrix diagonal with positive diagonal elements:

$$N_{\alpha j} M^{\tilde{\chi}^0}_{\alpha\beta} N_{\beta k} = m_{\tilde{\chi}^0_j} \delta_{jk}, \tag{C1}$$

where $m_{\tilde{\chi}^0_j} < m_{\tilde{\chi}^0_k}$ for $j < k$. In the basis

$$\psi_\alpha = \{\tilde{B}, \tilde{W}^0, \tilde{H}^a, \tilde{H}^b\}, \tag{C2}$$

the complex symmetric neutralino mass matrix has the form

$$M^{\tilde{\chi}^0}_{\alpha\beta} = \begin{pmatrix} M_1 & 0 & -m_Z \cos\beta \sin\theta_W & m_Z \sin\beta \sin\theta_W \\ 0 & M_2 & m_Z \cos\beta \cos\theta_W & -m_Z \sin\beta \cos\theta_W \\ -m_Z \cos\beta \sin\theta_W & m_Z \cos\beta \cos\theta_W & 0 & -\mu \\ m_Z \sin\beta \sin\theta_W & -m_Z \sin\beta \cos\theta_W & -\mu & 0 \end{pmatrix}. \tag{C3}$$

APPENDIX D: LOOP FUNCTIONS

In this appendix, we collect the different loop functions in the text:

$$H_2(x, y) = \frac{x \log x}{(1-x)(x-y)} + \frac{y \log y}{(1-y)(y-x)}, \tag{D1}$$

$$S_0(x) = \frac{4x - 11x^2 + x^3}{4(1-x)^2} - \frac{3x^3}{2(1-x)^3} \log x, \tag{D2}$$

$$f_1(x) = \frac{-7 + 5x + 8x^2}{6(1-x)^3} - \frac{2x - 3x^2}{(1-x)^4} \log x, \tag{D3}$$

$$f_2(x) = \frac{3x - 5x^2}{2(1-x)^2} + \frac{2x - 3x^2}{(1-x)^3} \log x, \tag{D4}$$

$$f_3(x) = \frac{1}{2(x-1)^3}(x^2 - 4x + 3 + 2\ln x), \tag{D5}$$

$$Y(x) = \frac{-3x^3 + 2x^2}{2(x-1)^4} \log x + \frac{8x^3 + 5x^2 - 7x}{12(x-1)^3}, \tag{D6}$$

$$W(x) = \frac{-32x^4 + 38x^3 + 15x^2 - 18x}{18(x-1)^4} \log x$$
$$+ \frac{-18x^4 + 163x^3 - 259x^2 + 108x}{36(x-1)^3}, \tag{D7}$$

$$f_5(x) = \frac{x}{1-x} + \frac{x}{(1-x)^2} \log x, \tag{D8}$$

$$f_6(x) = \frac{38x - 79x^2 + 47x^3}{6(1-x)^3} + \frac{4x - 6x^2 + 3x^4}{(1-x)^4} \log x, \tag{D9}$$

$$f_7(x) = \frac{52 - 101x + 43x^2}{6(1-x)^3} + \frac{6 - 9x + 2x^3}{(1-x)^4} \log x, \tag{D10}$$

$$c_0(m^2_1, m^2_2, m^2_3) = -\left[\frac{m^2_1 \log\frac{m^2_1}{\mu^2}}{(m^2_1 - m^2_2)(m^2_1 - m^2_3)} \right.$$
$$\left. + (m_1 \leftrightarrow m_2) + (m_1 \leftrightarrow m_3) \right], \tag{D11}$$

$$c_2(m_1^2, m_2^2, m_3^2) = \frac{3}{8} - \frac{1}{4}\left[\frac{m_1^2 \log\frac{m_1^4}{\mu^2}}{(m_1^2 - m_2^2)(m_1^2 - m_3^2)} + (m_1 \leftrightarrow m_2) + (m_1 \leftrightarrow m_3)\right], \quad \text{(D12)}$$

$$d_2(m_1^2, m_2^2, m_3^2, m_4^2)$$
$$= -\frac{1}{4}\left[\frac{m_1^4 \log\frac{m_1^4}{\mu^2}}{(m_1^2 - m_2^2)(m_1^2 - m_3^2)(m_1^2 - m_4^2)} + (m_1 \leftrightarrow m_2) + (m_1 \leftrightarrow m_3) + (m_1 \leftrightarrow m_4)\right]. \quad \text{(D13)}$$

[1] For a recent review, see A. Masiero and O. Vives, Annu. Rev. Nucl. Part. Sci. **51**, 161 (2001); New J. Phys. **4**, 4 (2002).

[2] G. D'Ambrosio, G. F. Giudice, G. Isidori, and A. Strumia, Nucl. Phys. **B645**, 155 (2002).

[3] M. Dine, R. G. Leigh, and A. Kagan, Phys. Rev. D **48**, 4269 (1993); G. G. Ross, L. Velasco-Sevilla, and O. Vives, Nucl. Phys. **B692**, 50 (2004); For a review and further references see G. G. Ross, in *TASI 2000*, edited by J. L. Rosner (World Scientific, New Jersey, 2001).

[4] K. S. Babu and C. F. Kolda, Phys. Rev. Lett. **84**, 228 (2000).

[5] S. R. Choudhury and N. Gaur, Phys. Lett. B **451**, 86 (1999).

[6] G. Isidori and A. Retico, J. High Energy Phys. 11 (2001) 001.

[7] C. Bobeth, T. Ewerth, F. Kruger, and J. Urban, Phys. Rev. D **66**, 074021 (2002).

[8] P. H. Chankowski and L. Slawianowska, Phys. Rev. D **63**, 054012 (2001).

[9] A. J. Buras, P. H. Chankowski, J. Rosiek, and L. Slawianowska, Phys. Lett. B **546**, 96 (2002).

[10] A. J. Buras, P. H. Chankowski, J. Rosiek, and L. Slawianowska, Nucl. Phys. **B659**, 3 (2003).

[11] G. Isidori and P. Paradisi, Phys. Lett. B **639**, 499 (2006).

[12] M. Carena, A. Menon, R. Noriega-Papaqui, A. Szynkman, and C. E. M. Wagner, Phys. Rev. D **74**, 015009 (2006).

[13] S. Baek, P. Ko, and W. Y. Song, J. High Energy Phys. 03 (2003) 054.

[14] A. Dedes, H. K. Dreiner, and U. Nierste, Phys. Rev. Lett. **87**, 251804 (2001).

[15] R. Arnowitt, B. Dutta, T. Kamon, and M. Tanaka, Phys. Lett. B **538**, 121 (2002).

[16] T. Ibrahim and P. Nath, Phys. Rev. D **67**, 016005 (2003).

[17] J. K. Mizukoshi, X. Tata, and Y. Wang, Phys. Rev. D **66**, 115003 (2002).

[18] A. Dedes, H. K. Dreiner, U. Nierste, and P. Richardson, hep-ph/0207026.

[19] H. Baer, C. Balazs, A. Belyaev, J. K. Mizukoshi, X. Tata, and Y. Wang, J. High Energy Phys. 07 (2002) 050.

[20] T. Blazek, S. F. King, and J. K. Parry, Phys. Lett. B **589**, 39 (2004).

[21] G. L. Kane, C. Kolda, and J. E. Lennon, hep-ph/0310042.

[22] J. R. Ellis, K. A. Olive, and V. C. Spanos, Phys. Lett. B **624**, 47 (2005).

[23] S. Baek, Y. G. Kim, and P. Ko, J. High Energy Phys. 02 (2005) 067.

[24] R. Dermisek, S. Raby, L. Roszkowski, and R. Ruiz De Austri, J. High Energy Phys. 04 (2003) 037.

[25] J. Ellis, K. A. Olive, Y. Santoso, and V. C. Spanos, J. High Energy Phys. 05 (2006) 063.

[26] A. Bartl, T. Gajdosik, E. Lunghi, A. Masiero, W. Porod, H. Stremnitzer, and O. Vives, Phys. Rev. D **64**, 076009 (2001).

[27] N. Polonsky and A. Pomarol, Phys. Rev. D **51**, 6532 (1995).

[28] L. E. Ibañez, D. Lust, and G. G. Ross, Phys. Lett. B **272**, 251 (1991); G. G. Ross, hep-ph/0411057.

[29] S. Martin and M. Vaughn, Phys. Rev. D **50**, 2282 (1994); Y. Yamada, Phys. Rev. D **50**, 3537 (1994); I. Jack and D. R. T. Jones, Phys. Lett. B **333**, 372 (1994).

[30] D. N. Spergel *et al.*, astro-ph/0603449.

[31] V. Abazov (D0 Collaboration), Phys. Rev. Lett. **97**, 021802 (2006).

[32] "Measurement of the Bs-Bs Oscillation Frequency," available at CDF's *B* physics web page, http://www-cdf.fnal.gov/physics/new/bottom/bottom.html.

[33] G. W. Bennett *et al.* (Muon $g - 2$ Collaboration), Phys. Rev. Lett. **92**, 161802 (2004).

[34] M. Iwasaki *et al.* (Belle Collaboration), Phys. Rev. D **72**, 092005 (2005).

[35] B. Aubert *et al.* (*BABAR* Collaboration), Phys. Rev. Lett. **93**, 081802 (2004).

[36] S. Eidelman *et al.* (Particle Data Group), Phys. Lett. B **592**, 1 (2004).

[37] CDF Collaboration, hep-ex/0507091.

[38] CDF Collaboration, Public note 8176; D0 Collaboration, note 5009-CONF.

[39] A. Dedes and A. Pilaftsis, Phys. Rev. D **67**, 015012 (2003).

[40] A. Brignole and A. Rossi, Phys. Lett. B **566**, 217 (2003).

[41] P. Paradisi, J. High Energy Phys. 02 (2006) 050.

[42] A. Masiero, P. Paradisi, and R. Petronzio, Phys. Rev. D **74**, 011701 (2006).

[43] A. M. Curiel, M. J. Herrero, W. Hollik, F. Merz, and S. Penaranda, Phys. Rev. D **69**, 075009 (2004).

[44] S. Kanemura, K. Matsuda, T. Ota, T. Shindou, E. Takasugi, and K. Tsumura, Phys. Lett. B **599**, 83 (2004).

[45] T. Ibrahim, P. Nath, and A. Psinas, Phys. Rev. D **70**, 035006 (2004).

[46] T. Ibrahim and P. Nath, Phys. Rev. D **71**, 055007 (2005).

[47] W. Hollik, S. Penaranda, and M. Vogt, Eur. Phys. J. C **47**, 207 (2006).

[48] A. Abulencia *et al.* (CDF Collaboration), Phys. Rev. Lett. **95**, 221805 (2005); **95**, 249905(E) (2005); V. M. Abazov

et al. (D0 Collaboration), Phys. Rev. Lett. **94**, 071802 (2005).

[49] G. Isidori and P. Paradisi, Phys. Rev. D **73**, 055017 (2006).

[50] A. J. Buras, P. H. Chankowski, J. Rosiek, and L. Slawianowska, Nucl. Phys. **B619**, 434 (2001).

[51] P. Gambino, U. Haisch, and M. Misiak, Phys. Rev. Lett. **94**, 061803 (2005).

[52] T. Huber, E. Lunghi, M. Misiak, and D. Wyler, Nucl. Phys. **B740**, 105 (2006).

[53] M. Ciuchini, G. Degrassi, P. Gambino, and G. F. Giudice, Nucl. Phys. **B527**, 21 (1998).

[54] A. J. Buras, A. Czarnecki, M. Misiak, and J. Urban, Nucl. Phys. **B631**, 219 (2002); A. J. Buras and M. Misiak, Acta Phys. Pol. B **33**, 2597 (2002).

[55] F. M. Borzumati and C. Greub, Phys. Rev. D **58**, 074004 (1998).

[56] F. M. Borzumati and C. Greub, Phys. Rev. D **59**, 057501 (1999).

[57] C. Bobeth, M. Misiak, and J. Urban, Nucl. Phys. **B567**, 153 (2000).

[58] G. Degrassi, P. Gambino, and G. F. Giudice, J. High Energy Phys. 12 (2000) 009.

[59] M. Carena, D. Garcia, U. Nierste, and C. E. M. Wagner, Phys. Lett. B **499**, 141 (2001).

[60] G. Degrassi, P. Gambino, and P. Slavich, Phys. Lett. B **635**, 335 (2006).

[61] S. Chen *et al.* (CLEO Collaboration), Phys. Rev. Lett. **87**, 251807 (2001).

[62] K. Abe *et al.* (Belle Collaboration), Phys. Lett. B **511**, 151 (2001).

[63] P. Koppunberg *et al.* (Belle Collaboration), Phys. Rev. Lett. **93**, 061803 (2004).

[64] B. Aubert *et al.* (*BABAR* Collaboration), Phys. Rev. D **72**, 052004 (2005).

[65] B. Aubert *et al.* (*BABAR* Collaboration), hep-ex/0507001.

[66] Heavy Flavor Averaging Group, hep-ex/0603003.

[67] T. Hurth, E. Lunghi, and W. Porod, Nucl. Phys. **B704**, 56 (2005).

[68] P. L. Cho, M. Misiak, and D. Wyler, Phys. Rev. D **54**, 3329 (1996).

[69] S. Bertolini, F. Borzumati, A. Masiero, and G. Ridolfi, Nucl. Phys. **B353**, 591 (1991).

[70] H. E. Haber and G. L. Kane, Phys. Rep. **117**, 75 (1985).

[71] T. Moroi, Phys. Rev. D **53**, 6565 (1996); **56**, 4424(E) (1997).

[72] G. W. Bennett (Muon Collaboration), Phys. Rev. D **73**, 072003 (2006).

[73] F. Jegerlehner, Nucl. Phys. B, Proc. Suppl. **126**, 325 (2004).

[74] ALEPH Collaboration, hep-ex/0602042.

[75] J. R. Ellis, K. A. Olive, Y. Santoso, and V. C. Spanos, Phys. Lett. B **565**, 176 (2003).

[76] G. Belanger, S. Kraml, and A. Pukhov, Phys. Rev. D **72**, 015003 (2005).

[77] D. M. Pierce *et al.*, Nucl. Phys. **B491**, 3 (1997).

[78] W. Porod (unpublished).

[79] G. Degrassi, P. Slavich, and F. Zwirner, Nucl. Phys. **B611**, 403 (2001).

[80] A. Brignole, G. Degrassi, P. Slavich, and F. Zwirner, Nucl. Phys. **B631**, 195 (2002).

[81] A. Brignole, G. Degrassi, P. Slavich, and F. Zwirner, Nucl. Phys. **B643**, 79 (2002).

[82] A. Dedes, G. Degrassi, and P. Slavich, Nucl. Phys. **B672**, 144 (2003).

[83] A. Dedes and P. Slavich, Nucl. Phys. **B657**, 333 (2003).

[84] B. C. Allanach, A. Djouadi, J. L. Kneur, W. Porod, and P. Slavich, J. High Energy Phys. 09 (2004) 044.

[85] C. Bobeth, A. J. Buras, F. Kruger, and J. Urban, Nucl. Phys. **B630**, 87 (2002).

[86] T. Goto, Y. Okada, Y. Shimizu, and M. Tanaka, Phys. Rev. D **55**, 4273 (1997); **66**, 019901(E) (2002).

[87] S. Baek, T. Goto, Y. Okada, and K.-i. Okumura, Phys. Rev. D **64**, 095001 (2001).

[88] T. Ibrahim and P. Nath, Phys. Rev. D **62**, 015004 (2000).

[89] P. B. Mackenzie, hep-ph/0606034.

[90] P. Ball and R. Fleischer, hep-ph/0604249.

[91] A. Dedes and B. T. Huffman, Phys. Lett. B **600**, 261 (2004).

[92] S. Asai (ATLAS and CMS Collaborations), Eur. Phys. J. direct C **4**, 17 (2002).

[93] A. Djouadi, hep-ph/0503173.

[94] H. Baer, J. Sender, and X. Tata, Phys. Rev. D **50**, 4517 (1994).

[95] T. Kon and T. Nonaka, Phys. Rev. D **50**, 6005 (1994).

[96] J. Sender, Phys. Rev. D **54**, 3271 (1996).

[97] W. Porod and T. Wöhrmann, Phys. Rev. D **55**, 2907 (1997); **67**, 059902(E) (2003).

[98] M. Hosch, R. J. Oakes, K. Whisnant, J. M. Yang, B. l. Young, and X. Zhang, Phys. Rev. D **58**, 034002 (1998).

[99] W. Porod, Phys. Rev. D **59**, 095009 (1999).

[100] C. Boehm, A. Djouadi, and Y. Mambrini, Phys. Rev. D **61**, 095006 (2000).

[101] D. Restrepo, W. Porod, and J. W. F. Valle, Phys. Rev. D **64**, 055011 (2001).

[102] A. Djouadi, M. Guchait, and Y. Mambrini, Phys. Rev. D **64**, 095014 (2001).

[103] S. P. Das, A. Datta, and M. Guchait, Phys. Rev. D **65**, 095006 (2002).

[104] W. Porod, Comput. Phys. Commun. **153**, 275 (2003).

[105] S. P. Das, A. Datta, and M. Guchait, Phys. Rev. D **70**, 015009 (2004).

[106] M. Muhlleitner, A. Djouadi, and Y. Mambrini, Comput. Phys. Commun. **168**, 46 (2005).

[107] T. Han, K. I. Hikasa, J. M. Yang, and X. Zhang, Phys. Rev. D **70**, 055001 (2004).

[108] K. Hikasa and M. Kobayashi, Phys. Rev. D **36**, 724 (1987).